Cell layer-specific expression of the homeotic MADS-box transcription factor PhDEF contributes to modular petal morphogenesis in petunia

Mathilde Chopy, Quentin Cavallini-Speisser, Pierre Chambrier, Patrice Morel, Jérémy Just, Véronique Hugouvieux, Suzanne Rodrigues Bento, Chloe Zubieta, Michiel Vandenbussche, Marie Monniaux

RESEARCH ARTICLE

Cell layer-specific expression of the homeotic MADS-box transcription factor PhDEF contributes to modular petal morphogenesis in petunia

Mathilde Chopy[1,2], Quentin Cavallini-Speisser[1], Pierre Chambrier[1] , Patrice Morel[1], Jérémy Just[1] , Véronique Hugouvieux[3], Suzanne Rodrigues Bento[1], Chloe Zubieta[3], Michiel Vandenbussche [1,*] and Marie Monniaux [1,*]

[1] Laboratoire de Reproduction et Développement des Plantes, Université de Lyon, ENS de Lyon, UCB Lyon 1, CNRS, INRAE, 69007 Lyon, France.

[2] Current address: Institute of Plant Sciences, University of Bern, Altenbergrain 21, Bern, CH-3013, Switzerland.

[3] Laboratoire de Physiologie Cellulaire et Végétale, Université Grenoble-Alpes, CNRS, CEA, INRAE, IRIG-DBSCI, 38000 Grenoble, France.

Short title: Role of cell layers in petal development

One-sentence summary: The expression of B-class homeotic MADS-box transcription factor *PhDEF* in different cell layers drives petunia petal tube or limb development.

*** Corresponding authors:** Michiel Vandenbussche (michiel.vandenbussche@ens-lyon.fr) and Marie Monniaux (marie.monniaux@ens-lyon.fr)

The authors responsible for distribution of materials integral to the findings presented in this article in accordance with the policy described in the Instructions for Authors (https://academic.oup.com/plcell/pages/General-Instructions) are: Marie Monniaux (marie.monniaux@ens-lyon.fr) and Michiel Vandenbussche (michiel.vandenbussche@ens-lyon.fr).

ABSTRACT

Floral homeotic MADS-box transcription factors ensure the correct morphogenesis of floral organs, which are organized in different cell layers deriving from distinct meristematic layers. How cells from these distinct layers acquire their respective identities and coordinate their growth to ensure normal floral organ morphogenesis is unresolved. Here, we studied petunia (*Petunia x hybrida*) petals that form a limb and tube through congenital fusion. We identified petunia mutants (periclinal chimeras) expressing the B-class MADS-box gene *DEFICIENS* in the petal epidermis or in the petal mesophyll, called *wico* and *star*, respectively. Strikingly, *wico* flowers form a strongly reduced tube while their limbs are almost normal, while *star* flowers form a normal tube but greatly reduced and unpigmented limbs, showing that petunia petal morphogenesis is highly modular. These mutants highlight the layer-specific roles of PhDEF during petal development. We explored the link between PhDEF and petal pigmentation, a well-characterized limb epidermal trait. The anthocyanin biosynthesis pathway was strongly down-regulated in *star* petals, including its major regulator *ANTHOCYANIN2 (AN2)*. We established that PhDEF directly binds to the *AN2* terminator *in vitro* and *in vivo*, suggesting that PhDEF might regulate *AN2* expression and therefore petal epidermis pigmentation. Altogether, we show that cell layerspecific homeotic activity in petunia petals differently impacts tube and limb development, revealing the relative importance of the different cell layers in the modular architecture of petunia petals.

IN A NUTSHELL

Background: Petals are not only beautiful, but they are also very important floral organs that have co-evolved with different animal visitors to ensure pollination. This long co-evolution produced many complex petal shapes. In the case of *Petunia*, the fused petals are organized in two domains, the tube and the limb; this influences the interaction of the flower with hawkmoths, hummingbirds, or bees. Petal identity genes, such as *PhDEFICIENS* (*PhDEF*), trigger petal development resulting in mature petals. However, the mechanisms by which those genes drive complex petal shape with tube and limb, are unclear.

Question: Petals are formed of cell layers: the epidermis and the internal cells. In a wild-type flower, the petal identity gene *PhDEF* is expressed in all cell layers. But what happens if *PhDEF* expression is restricted to a specific cell layer? In other words, we wanted to investigate the layer-specific contribution of *PhDEF* in petal tube and limb development.

Findings: By chance, we obtained the perfect material to address this question: Two categories of *Petunia hybrida* mutants (chimeras) expressing *PhDEF* exclusively in the petal epidermis or in the inner cells, called *wico* and *star*, respectively. The resulting flowers displayed dramatically different limb and tube shape (see picture): *wico* flowers form a strongly reduced tube while their limb is almost normal, and *star* flowers form a normal tube but a very reduced limb. This suggests that

petunia petal morphogenesis is highly modular, and depends on the cell layer-specific expression of *PhDEF*.

Next steps: This study is a first step towards understanding the link between *PhDEF* and complex petal development. A major future challenge is to identify the genes acting downstream of the petal identity genes, at the tissue (epidermis vs internal cells) and organ (limb vs tube) scales.

INTRODUCTION

All plant aerial organs derive from clonally distinct layers, named L1, L2 and L3 in the shoot apical meristem (SAM) (Satina et al., 1940). Within the L1 and L2 layers, cells divide anticlinally, thereby maintaining a clear layered structure in all aerial organs produced by the SAM (Meyerowitz, 1997; Stewart and Burk, 1970; Scheres, 2001). Already at the embryonic stage, meristematic cell layers express different genes and have distinct identities (Abe et al., 1999; Lu et al., 1996), that are maintained in the adult SAM (Yadav et al., 2014). During flower development, floral organ identity will be appended on top of layer identity by the combinatorial expression of homeotic floral genes, most of which are MADS-box genes (Coen and Meyerowitz, 1991; Schwarz-Sommer et al., 1990). How these master floral regulators specify all floral organ features, such as organ size, shape, pigmentation, and cellular properties, while maintaining layer-specific identities, is unknown.

Petals are often the most conspicuous organs of the flower, and they display a tremendous diversity in size, shape and pigmentation across flowering plants (Moyroud and Glover, 2017). Floral organ identity is specified by a combination of A-, B- and C-class identity genes as proposed by the classical ABC model established in Arabidopsis (*Arabidopsis thaliana*) and snapdragon (*Antirrhinum majus*), and B-class genes are particularly important for petal identity (Coen and Meyerowitz, 1991; Schwarz-Sommer et al., 1990; Morel et al., 2017). B-class proteins, belonging to MADS-box transcription factors, are grouped in the DEF/AP3 and the GLO/PI subfamilies, named after the snapdragon/Arabidopsis B-class proteins DEFICIENS/APETALA3 and GLOBOSA/PISTILLATA (Purugganan et al., 1995; Theißen et al., 1996). These proteins act as obligate heterodimers consisting of one DEF/AP3 and one GLO/PI protein, together with other MADS-box transcription factors of the SEPALLATA subfamily (Melzer et al., 2009), and this complex activates the expression of *DEF/AP3* and *GLO/PI* genes for maintenance of high expression levels throughout petal and stamen development (Tröbner et al., 1992).

In petunia (*Petunia x hybrida*, abbreviated *Ph* for gene names), gene duplication has generated four B-class genes, namely *PhDEF* (*DEFICIENS*) and *PhTM6 (TOMATO MADS-BOX GENE6)* belonging to the *DEF/AP3* subfamily, and *PhGLO1* (*GLOBOSA1*) and *PhGLO2* (*GLOBOSA2*) belonging to the *GLO/PI* subfamily (Vandenbussche et al., 2004; Rijpkema et al., 2006; van der Krol et al., 1993; Angenent et al., 1992). Mutating the two members of each subfamily (*phdef phtm6* or *phglo1 phglo2* double mutants) results in a classical B-function mutant phenotype with homeotic transformation of petals into sepals and stamens into carpels (Vandenbussche et al., 2004; Rijpkema et al., 2006). Additionally, gene copies within the *DEF/AP3*

subfamily have diverged in function: while *PhDEF* exhibits a classical B-class expression pattern largely restricted to developing petals and stamens, *PhTM6* is atypically expressed in stamens and carpels, and its upregulation depends on the petunia C-function genes (Rijpkema et al., 2006; Heijmans et al., 2012a). As a consequence, the single *phdef* mutant displays a homeotic conversion of petals into sepals, while the stamens are normal due to functional redundancy with *PhTM6* (Rijpkema et al., 2006). The petunia *phdef* mutant is therefore an interesting model to study the mechanism of petal identity specification alone since it displays a single-whorl complete homeotic transformation, which is quite rare for floral homeotic mutants that generally show defects in two adjacent whorls.

Flowers from the *Petunia* genus develop five petals, that arise as individual primordia and fuse congenitally (Vandenbussche et al., 2009). Mature petals are fully fused and the corolla is organized in two distinct domains: the tube and the limb. Variation in the relative size of the tube and the limb is observed among wild species of *Petunia*, where flowers with a long tube grant nectar access to long-tongued hawkmoths or hummingbirds, while wide and short tubes are easily accessible to bees (Galliot et al., 2006). The short- and long-tube species cluster separately on a phylogeny of wild *Petunia* species, and the short-tube phenotype is likely the ancestral one (Reck-Kortmann et al., 2014). Pollinator preference assays and field observations have confirmed that tube length and limb size are discriminated by pollinators and thereby might play a role in reproductive isolation, together with multiple other traits of the pollination syndromes such as limb pigmentation or volatile emission (Venail et al., 2010; Hoballah et al., 2007; Galliot et al., 2006). Tube and limb therefore appear to act as different functional modules in the petunia flower.

Although the petunia petal tube and limb seem to play important ecological roles, the mechanisms driving their development are mostly unknown. Tube and limb develop as relatively independent entities in flowers from the Solanaceae family, to which petunia belongs: for instance, tube length and limb width are uncorrelated traits in intra-specific crosses performed in *Nicotiana* or *Jaltomata* (Bissell and Diggle, 2008; Kostyun et al., 2019). Moreover, tube and limb identities can be acquired independently: this is strikingly observed in the petunia *blind* mutant, a partial A-class mutant that forms an almost wild-type tube topped by functional anthers, due to ectopic C-class activity in the second whorl (Cartolano et al., 2007). Apart from the petal identity genes, the molecular players involved in petunia tube or limb morphogenesis are mostly unknown. General growth factors affect petal development as a whole (both tube and limb) together with other vegetative or reproductive traits (Vandenbussche et al., 2009; Terry et al., 2019; Brandoli et al.,

2020), but very few genes have been found to specifically affect growth of one subdomain of the petal (Zenoni et al., 2004). Therefore, the mechanisms of petunia tube and limb morphogenesis remain to be fully explored.

In contrast, the genetic and molecular bases of petunia petal pigmentation are extremely well characterized, thanks to the plethora of mutants that have been isolated over decades of breeding and research (Bombarely et al., 2016; Tornielli et al., 2009). Petunia limb pigmentation is mainly due to the accumulation of anthocyanins in the vacuole of adaxial epidermal cells. Briefly, the earliest steps of anthocyanin production are ensured by a MBW regulatory complex composed of an R2R3-MYB transcription factor (either ANTHOCYANIN2 (AN2), AN4, DEEP PURPLE (DPL) or PURPLE HAZE), a bHLH transcription factor (AN1 or JAF13), and a WD-40 repeat protein (AN11), which drives the expression of anthocyanin biosynthesis enzymes and proteins involved in vacuolar acidification of epidermal cells (Albert et al., 2011; de Vetten et al., 1997; Spelt et al., 2000; Quattrocchio et al., 1998, 1999, 1993). How this pathway is activated, after regulators such as PhDEF have specified petal identity, has not been elucidated so far.

In this work, we present petunia flowers with strongly affected tube or limb development, that we respectively named *wico* and *star*, and that spontaneously arose from *phdef-151* mutant plants. We provide genetic and molecular evidence that both of these flower types are periclinal chimeras, resulting from the layer-specific excision of the transposon inserted into the *PhDEF* gene, restoring *PhDEF* activity either in the epidermis or in the mesophyll of the petal. The *star* and *wico* phenotypes indicate that in the petunia petal, the epidermis mainly drives limb morphogenesis while the mesophyll mainly drives tube morphogenesis. This is seemingly different from previous studies in snapdragon flowers, another species with fused petals, where *def* periclinal chimeras indicated that epidermal *DEF* expression was making a major contribution to overall petal morphology (Perbal et al., 1996; Vincent et al., 2003; Efremova et al., 2001). We characterized in detail the *star* and *wico* petal phenotypes at the tissue and cellular scale, and found evidence for non-cell-autonomous effects affecting cell identity between layers. We sequenced the total petal transcriptome from wild-type (wt), *wico* and *star* flowers at three developmental stages, and we found that a large proportion of the genes involved in anthocyanin production were downregulated in *star* petal samples, as could be expected from their white petals. We further showed, by gel shift assay and chromatin immunoprecipitation, that PhDEF binds to the terminator region of *AN2*, thereby possibly regulating its expression and triggering the first steps of limb pigmentation. Our results and our unique flower material promise to improve our understanding of tube and limb

169 morphogenesis in petunia, and address the broader question of how organ identity and cell layer
170 identity overlap during organ development.
171

RESULTS

Spontaneous appearance of two phenotypically distinct classes of partial revertants from the *phdef-151* locus

Previously described null alleles for the *PhDEF* gene (also named *GP* or *pMADS1*) were obtained by either ethyl methanesulfonate (EMS) mutagenesis (de Vlaming et al., 1984; Rijpkema et al., 2006) or by γ-radiation (van der Krol et al., 1993). Because neither of these alleles were straightforward to genotype in a heterozygous state, we screened our sequence-indexed *dTph1* transposon mutant population in the W138 genetic background (Vandenbussche et al., 2008) for other insertions into *PhDEF*. We identified a mutant allele named *phdef-151*, referring to the *dTph1* insertion 151 bp downstream of the ATG in the first exon of the *PhDEF* gene, predicted to fully disrupt the MADS-domain in the protein sequence by premature termination of the first exon due to multiple stop codons in the different reading frames of *dTph1*. As observed for previously identified *phdef* null alleles, *phdef-151* flowers display a complete homeotic conversion of petals into sepals, while heterozygous or homozygous wild-type siblings display red-coloured wild-type petals (Fig. 1A-C). *phdef-151* is thus very likely a null mutant allele.

While growing homozygous *phdef-151* individuals during several seasons, we repeatedly observed the spontaneous appearance of inflorescence side branches that developed flowers with a partial restoration of petal development (Figure 1, Supplemental Figure S1), suggesting excision of the *dTph1* transposon from the *phdef-151* allele specifically in these side branches. Remarkably, these partially revertant flowers could be classified as belonging to either one of two contrasting phenotypic classes, that we named *star* and *wico*, and that could even occur simultaneously in different branches on the same plant (Fig. 1A). For both phenotypic classes, we obtained more than 15 independent reversion events. The *star* flowers (Fig. 1D-F), named in reference to their star-shaped petals, grow an elongated tube similar to wild-type (wt) flowers, but their limbs are underdeveloped: they appear to mainly grow around the mid-vein with strongly reduced lateral expansion, hence losing the typical round shape of wt limb. Moreover, they have almost white petals, suggesting strongly reduced accumulation of anthocyanins.

We quantified the changes in flower morphology (Fig. 1K-N) and found that total limb area was reduced almost 5-fold in *star* flowers (Fig. 1M). In contrast, total tube length was only slightly reduced (by 19%) in *star* as compared to wt (Fig. 1L), and this was mainly due to a reduction in length of domain D1, corresponding to the part of the tube fused with stamens (as defined in (Stuurman et al., 2004), Fig. 1K), while length of the rest of the tube (domain D2) remained

unchanged (Fig. 1L, Supplemental Figure S2). As a result, the ratio between limb area and tube length, which we use as a simple measure for overall corolla morphology, is reduced about 4-fold in *star* flowers as compared to wt (Fig. 1N). In addition, we occasionally observed fully pigmented secondary revertant sectors of various sizes in the *star* genetic background, in some cases leading to the development of a single wt-like petal in a *star* flower background (Fig. 1J). These revertant sectors, observed multiple times, always exhibited simultaneous restoration of pigmentation and normal petal limb growth patterns, demonstrating that the strongly reduced pigmentation in *star* petals was due to impaired PhDEF function, and not to an additional mutation in the pigmentation pathway.

The *wico* flowers, named after their wide corolla, grow round-shaped and pigmented limbs while their tube remains underdeveloped (Fig. 1G-I). Limb pigmentation ranged from pink to bright red, and green sepaloid tissue was observed around the mid-veins, commonly well visible in all *wico* flowers on the abaxial side of the petals (see for instance Supplemental Figure S1E). Total tube length was reduced about 3-fold in *wico* flowers, with domain D1 being absent since stamens were totally unfused to the tube (Supplemental Figure S2), while domain D2 was significantly reduced in size compared to wild type (Fig. 1L). Limb area was also about 2-fold reduced in *wico* as compared to wt flowers (Fig. 1M), but the ratio between limb area and tube length was higher than in wt flowers (Fig. 1N), indicating the larger contribution of limb tissue to total corolla morphology in *wico* flowers. In summary, the *star* flowers form an almost normal tube but small, misshaped and unpigmented limbs, while the *wico* flowers form almost normally shaped and pigmented limbs but a tube strongly reduced in length. These contrasting phenotypes suggest that tube and limb development can be uncoupled in petunia flowers, at least to some degree.

The *star* and *wico* flowers result from excision of the *dTph1* transposon from the *phdef-151* locus

Reversion of a mutant phenotype towards a partial or a complete wt phenotype is classically observed in unstable transposon insertion mutant alleles. In the petunia W138 line from which *phdef-151* originates, the *dTph1* transposon is actively transposing (Gerats et al., 1990). We assumed therefore that the *star* and *wico* flowers were caused by the excision of *dTph1* from the *PhDEF* locus. *dTph1* transposition is generally accompanied by an 8-bp duplication of the target site upon insertion, and excision can have various outcomes depending on the length and nature of the remaining footprint (van Houwelingen et al., 1999). Hence, we first hypothesized that the

distinct *star* and *wico* phenotypes were caused by different types of alterations of the *PhDEF* coding sequence after the excision of *dTph1*.

To test this hypothesis, we characterized the *phdef-151* locus from in total 14 *star* and 14 *wico* independent reversion events (Figure 2). For this, we amplified part of the *PhDEF* locus (Fig. 2A) and specifically sequenced the fragments resulting from *dTph1* excision in *phdef-151*, *star* and *wico* second whorl organs (Fig. 2B-C). In *phdef-151,* the *dTph1*-excised alleles were always out-of-frame, with either 7 or 8 additional nucleotides as compared to the wt sequence. Due to a reading frame shift, both of these alleles are expected to produce an early truncated protein likely not functional (Fig. 2C), in line with the normal *phdef* mutant phenotype observed in these plants. In contrast, in both *star* and *wico* flowers we could find either wt sequences (found 1 time and 3 times independently in *star* and *wico* flowers respectively) or in-frame footprint alleles consisting of various additions of 6 nucleotides (alleles further named *PhDEF+6*, found 13 times and 11 times independently in *star* and *wico* flowers respectively, Fig. 2C). These last insertions are predicted to result in proteins with 2 additional amino-acids inserted towards the end of the DNA-binding MADS domain (Fig. 2C). Together, these results demonstrate that *wico* and *star* revertant flowers depend on the presence of an in-frame *def-151* derived excision allele that partially restores petal development.

However, and in contrast to our initial expectations, there was no association between the sequence of the locus after excision and the phenotype of the flower, and both *star* and *wico* flowers could be found with a wt *PhDEF* excision allele or with an identical *PhDEF+6* allele (e.g. the 6-bp GTCTGG footprint allele was frequently found both in *wico* and *star* flowers). This indicates that the phenotypic difference between the *star* and *wico* flowers cannot be explained by a differently modified *PhDEF* sequence after *dTph1* excision. Secondly, since the *phdef* mutation is fully recessive (Vandenbussche et al., 2004), the presence of one transposon mutant allele combined with the wt revertant sequence, normally should lead to wt flowers. Together this implied that another molecular mechanism was causing the difference between *wico* and *star* flowers.

The *wico* flowers are L1 periclinal chimeras

Excision of *dTph1* from a gene can occur at different times during plant development: if happening at the zygotic stage, then the whole plant will have a *dTph1*-excised allele. If excision occurs later, this will result in a genetic mosaic (chimera) with a subset of cells carrying the *dTph1* insertion at the homozygous state and others having a *dTph1*-excised allele. This typically leads to branches or

flowers with a wt phenotype on a mutant mother plant (assuming a recessive mutation). Furthermore, since all plant organs are organized in clonally-independent cell layers, excision can happen in one cell layer only, thereby creating a periclinal chimera, *i.e.* a branch or flower where cell layers have different genotypes (Frank and Chitwood, 2016; De Keukeleire et al., 2001).

Analyzing the progeny of *wico* flowers suggested that they were periclinal chimeras, since the *wico* phenotype was not heritable (in consequence, they had to be maintained by cuttings of revertant branches). Instead, we found that the progeny of the *wico* flowers displayed a *phdef* mutant phenotype at a proportion close to 100%, undistinguishable from the parental *phdef-151* allele (Table 1). This suggested that the gametes generated by the *wico* flowers exclusively carried the mutant *phdef-151* allele, hence resulting in homozygous *phdef-151* mutants in the progeny. Gametes are exclusively derived from the L2 layer in flowering plants (Tilney-Bassett, 1986), therefore indicating that L2-derived germ cells were homozygous mutant for *phdef-151* in *wico* flowers, which should result in a *phdef* phenotype if the epidermal tissue had the same genotype. This discrepancy suggested that the L1 layer of *wico* flowers was probably carrying a functional *PhDEF* allele.

To test this hypothesis, we localized the *PhDEF* transcript in *wico* flowers by *in situ* hybridization (Figure 3, Supplemental Figure S3). In wt flowers, the *PhDEF* transcript was first detected in the stamen initiation domain, then shortly after in incipient stamen and petal primordia (Fig. 3A, B). At all stages observed, *PhDEF* expression appeared quite homogeneous in all cell layers of the organs, with a stronger expression in the distal part of the petal at later stages of development (Fig. 3C, Supplemental Figure S3). In contrast, in *wico* flowers *PhDEF* expression was restricted to the L1 and epidermis, all throughout petal development (Fig. 3G-I, Supplemental Figure S3). Therefore, we conclude that *wico* flowers are the result of an early *dTph1* excision event in one cell from the L1 meristematic layer, resulting in a chimeric flower expressing *PhDEF* only in the epidermis (L1-derived cells) of petals. *Wico* flowers are therefore L1-periclinal chimeras.

The *star* flowers are L2 periclinal chimeras

Similarly, we analyzed the progeny of the *star* flowers, and the *star* phenotype was also not heritable, and hence maintained by cuttings of revertant branches. The progeny of the *star* flowers with a *PhDEF+6* allele yielded three different phenotypic classes (in a proportion close to 1:1:2; Table 1): plants displaying a *phdef* phenotype, plants having wt flowers, and plants carrying flowers

with a wild-type architecture but with altered pigmentation, further referred to as « pink wt » (Supplemental Figure S4).

We genotyped the *PhDEF* locus in plants descendant from one *star* parent and carrying flowers with a wt architecture (Supplemental Table S1). We found that all plants with a pink wt phenotype were heterozygous with an out-of-frame *phdef* allele and an in-frame *PhDEF+6* allele, while fully red wt flowers had in-frame *PhDEF+6* alleles at the homozygous state. This indicates that the PhDEF protein with 2 additional amino acids is not 100% fully functional, as it leads to a reduction in limb pigmentation when combined with an out-of-frame allele. The fact that it can ensure normal petal development when at the homozygous state indicates that this is dosage dependent. In summary, the segregation ratio shows that the *star* gametes carried either the *phdef-151* allele or an in-frame *PhDEF* allele at a 1:1 ratio, and hence that the germ cells generating these gametes were heterozygous for these two alleles. This suggested that in *star* flowers, the L2 layer was carrying a functional *PhDEF* allele (either wild-type *PhDEF* or *PhDEF+6*) while the L1 layer was homozygous mutant for *phdef-151*.

In support of this, in *star* flowers *PhDEF* expression was absent from the L1 and epidermis (Fig. 3D-F, Supplemental Figure S3). At the petal margins, underlying layers were also devoid of *PhDEF* expression (Fig. 3F), which likely corresponds to the restricted petal area where cells of L1 origin divide periclinally and invade the mesophyll (Satina and Blakeslee, 1941). Therefore, we conclude that *star* flowers are the result of an early *dTph1* excision event in one cell from the L2 meristematic layer, resulting in a chimeric flower expressing *PhDEF* only in the mesophyll (L2-derived cells) of petals. *Star* flowers are therefore L2-periclinal chimeras. Considering the *star* and *wico* phenotypes, we can conclude that the petal epidermis is the main driver for limb morphogenesis (growth, shape and pigmentation), while the mesophyll mainly drives tube morphogenesis (growth and shape).

Non-cell-autonomous effects of layer-specific *PhDEF* expression on cell identity

Having determined the genetic basis of the *star* and *wico* phenotypes, we next wondered how layer-specific *PhDEF* expression affects the determination of cell identity, in the layer where *PhDEF* is expressed (cell-autonomous effect) but also in the layer devoid of *PhDEF* expression (non-cell-autonomous effect). For this, we observed petal adaxial epidermal cells by scanning electron microscopy, and mesophyll cells on petal cross-sections, in wt petals and sepals, and in *star* and *wico* petals (Figure 4).

On the adaxial side of the wt petal (Fig. 4A), cells from the limb are round and conical as in many angiosperm petal limbs, while cells from the tube are elongated with a central cone (Fig. 4B) (Cavallini-Speisser et al., 2021). In contrast, the adaxial epidermis of wt sepals (indistinguishable from *phdef-151* second whorl organs) displays typical leaf-like features (Morel et al., 2019), with puzzle-shaped cells interspersed with stomata and trichomes (Fig. 4B). Epidermal cell identity can thus be clearly determined on the basis of cell shape. In *wico* petals, epidermal limb cells are conical, similar to wt cells from the same area, although marginally bigger (Fig. 4B, D). In contrast, cells from the tube, albeit displaying a similar shape to wt cells, are strongly reduced in length (Fig. 4B, E), suggesting that a defect in cell elongation is at least partly responsible for tube length reduction in *wico* petals.

In *star* petal tubes, epidermal cells have a similar appearance as in a wt petal tube but are slightly less elongated (Fig. 4B, E). In contrast, epidermal cells from the *star* limb are slightly bulging cells, more or less roundish and about 3-times larger than wt conical cells (Fig. 4D). Pigmented revertant sectors on star flowers (resulting from an additional *dTph1* excision in the epidermis) allow the immediate comparison between *star* and wt epidermal cells on a single sample, confirming the difference in conical cell size, shape and colour (Supplemental Figure S5). Moreover, the *star* limb adaxial epidermis occasionally forms trichomes (Supplemental Figure S5), a feature that is normally not observed in the wt limb adaxial epidermis. Altogether, these observations suggest that epidermal cells from *star* limb have an intermediate identity between petal and sepal cells.

Mesophyll cell identity was investigated by analyzing petal cross-sections stained with toluidine blue (Fig. 4C). In the wt petal, mesophyll cells are loosely arranged, big and round in the tube, and small and elongated in the limb. Sepal mesophyll cells are bigger than petal mesophyll cells, and they display the typical leaf mesophyll organization with an upper palisade layer (elongated and parallel cells) and a lower spongy layer (dispersed cells). Hence mesophyll cell size, shape and tissue-level organization are characteristic features allowing to distinguish between sepal and petal mesophyll tissue.

In *star* petals, the mesophyll strongly resembles a wt petal mesophyll in its organization, however cells are bigger and more densely packed in the tube, suggesting that *PhDEF* activity in the L2 layer is not entirely sufficient to specify normal mesophyll formation in the tube, which might be linked to the slightly reduced size of the tube of *star* flowers (Fig. 1L). In *wico* petals, mesophyll cells appeared very similar to wt and their organization was clearly distinct from the one

found in sepals since no palisade layer was observed. However, peeling the epidermis from *wico* limb revealed that the underlying mesophyll harbored chloroplasts, similar to a sepal mesophyll and in striking contrast with the white mesophyll of wt petal limb (Fig. 4F). Thus, the *phdef* mutant mesophyll in *wico* flowers has an intermediate identity between sepal and petal. In summary, our results show that for most features, *PhDEF* directs petal cell identity autonomously, and that non-autonomous effects also influence cell identity across layers. The interpretation of these effects is summarized in Supplemental Figure S6. In contrast, the observation of *star* revertant sectors (Supplemental Figure S5) revealed that cell identity is entirely defined autonomously within the epidermal layer, since a sharp transition in cell pigmentation, size and shape is observed in these sectors (Supplemental Figure S5). This suggests that different processes are at stake for cell-cell communication of petal identity across and within layers.

The physical nature of the non-autonomous effects that we identified remains unknown. Our *in situ* hybridization assays show that the mRNA of *PhDEF* is not mobile, but our attempts to localize the PhDEF protein by immuno-histochemistry have been unsuccessful; hence we do not know if the PhDEF protein itself might move between petal layers. Alternatively, and non-exclusively, other molecular players or mechanical signals might mediate information between layers.

Transcriptome sequencing of *star* and *wico* petals

To better understand the molecular basis for the *star* and *wico* phenotypes, we performed RNA-Seq on total petal tissue at three developmental stages, including wt and *phdef-151* samples (Figure 5). We chose an early stage (stage 4 as defined in (Reale et al., 2002)), an intermediate stage (stage 8) when tube length is at half its final size, and a late stage (stage 12) before limb is fully expanded (Fig. 5A). For *phdef-151* we only sequenced second-whorl sepal tissue at stage 12 (before anthesis). Principal component analysis showed that developmental stage is the first contributor to variation in gene expression, while genotype corresponds to the second axis of variation (Fig. 5B). All genotypes clustered separately except *wico* and wt samples which were highly similar at the two later stages. We analyzed one-to-one differential gene expression between mutant and wt samples with DESeq2 (Love et al., 2014) and we found on average 5,818 differentially expressed genes (DEGs) in *phdef-151*, as compared to 1,854 and 1,115 DEGs in *star* and *wico* respectively, when averaging for all stages (Fig. 5C, Supplemental Dataset S1).

There were generally more upregulated genes than downregulated ones in mutant or chimeric genotypes, and the number of DEGs increased as development progressed in the petal in both *star* and *wico* (Fig. 5C). At stage 12, a large proportion of DEGs (58-61%) in *wico* or *star* petals were also differentially expressed in *phdef-151* (Fig. 5D), as expected since *wico* and *star* flowers are mutant for *PhDEF* in one cell layer. Genes uniquely differentially expressed in *star* or *wico* flowers represented 36% of DEGs for each, and only 16-29% of DEGs were jointly differentially expressed in *star* and *wico* flowers, consistent with the very different phenotypes of these flowers. These proportions indicate that the *star* and *wico* phenotypes are mostly subtended by the differential expression of sets of genes also differentially expressed in *phdef-151*, together with the differential expression of a unique set of genes for each genotype.

In *star* and *wico* petals, we found that *PhDEF* was down-regulated about two-fold at all stages (Supplemental Figure S7), as expected since *PhDEF* is expressed in one cell layer only. In contrast, *PhTM6* was not differentially expressed in *star* and *wico* nor in *phdef-151* (Supplemental Figure S7), as expected since this atypical B-class gene is mostly expressed in stamens and carpels and its upregulation depends on the C-function genes (Rijpkema et al., 2006; Heijmans et al., 2012b). Unexpectedly, we observed that the B-class genes *PhGLO1* and *PhGLO2* were not down-regulated in *wico* petals, and only modestly in *star* petals, although their expression was almost null in the *phdef-151* mutant (Supplemental Figure S7). The fact that *PhGLO1* and *PhGLO2* expression does not strictly mirror the expression of *PhDEF* in *star* and *wico* petals, which is what we would have expected since the B-class heterodimers are known to activate their own expression, suggests that *PhGLO1* and *PhGLO2* expression is not entirely dependent on the B-class heterodimeric complexes, in particular in the epidermal layer of the petal.

PhDEF directly binds *in vivo* to the terminator region of *AN2*, encoding a major regulator of petal pigmentation

The *star* and *wico* periclinal chimeras have revealed layer-specific roles of PhDEF in the establishment of petal identity and petal development. More specifically, the major layer-specific phenotypes that we have identified are petal pigmentation, conical cell formation and limb growth (controlled by the epidermal-specific expression of *PhDEF*), and tube growth (controlled by the mesophyll-specific expression of *PhDEF*). Therefore, our chimeras show the potential to further explore the exact nature of the link between layer-specific *PhDEF* activity and layer-specific phenotypes. As a proof-of-concept, we explored if PhDEF could directly control petal pigmentation

426 in the limb epidermis. Pigmentation appeared to us as a trait of choice, since its regulatory and
427 biosynthetic factors are well described, while this was not the case for the other traits mentioned
428 above. Moreover, the absence of pigmentation in *star* petals, the restoration of pigmentation in L1-
429 revertant sectors and the phenotype of the pink wt flowers all converged to a direct link between
430 *PhDEF* expression in the epidermis and petal pigmentation.

431 For this, we examined the 451 genes down-regulated in both *phdef-151* and *star* samples (at
432 any stage) but not differentially expressed in *wico* samples (Supplemental Dataset S2), and we
433 found 23 anthocyanin-related genes in this gene set (Supplemental Figure S7), out of a total of 42 in
434 the whole genome, which constitutes an exceptionally high enrichment for this gene function ($p <$
435 0.001, Fisher's exact test). We paid particular attention to the genes possibly involved in the first
436 steps of anthocyanin production, ie encoding proteins involved in the MBW complexes activating
437 anthocyanin biosynthesis (AN1, AN2, AN4, AN11, JAF13, DPL and PURPLE HAZE). We found
438 that *AN1*, *AN2*, *DPL* and *JAF13* were downregulated both in *phdef-151* and *star* samples
439 (Supplemental Figure S7, Supplemental Dataset S2). DPL is involved in the limb venation pattern
440 (Albert et al., 2011; Zhang et al., 2021) and JAF13 has only a moderate contribution to limb
441 pigmentation (Bombarely et al., 2016), therefore we decided to focus our attention on the two major
442 activators of anthocyanin biosynthesis AN1 and AN2 (Figure 6).

443 Indeed, the *an1* mutant has fully white petals and the *an2* mutant has strongly reduced limb
444 pigmentation (Quattrocchio et al., 1999; Spelt et al., 2000). Furthermore, AN2 was shown to act as
445 an upstream activator of *AN1* since overexpressing *AN2* in petunia leaves is sufficient to activate
446 *AN1* expression, and for anthocyanins to accumulate (Quattrocchio et al., 1998; Spelt et al., 2000).
447 We observed that both genes were already expressed at stage 4 of wt petal development, before any
448 pigmentation is visible, and their expression levels strongly increased from stage 4 to stage 12,
449 while both being strongly downregulated in *star* petals and *phdef-151* second whorl organs, but not
450 in *wico* flowers (Fig. 6A, B). *AN2* was expressed at higher levels than *AN1* at all stages, consistent
451 with its most upstream role in the anthocyanin pigmentation pathway.

452 We aimed to test if PhDEF could directly bind to *AN1* and *AN2* genomic sequence,
453 potentially to regulate their expression. For this, we first attempted to predict PhDEF binding on the
454 genomic sequences of *AN1* and *AN2*. We used the high-quality transcription factor (TF) binding
455 profile database Jaspar (Fornes et al., 2020; Sandelin et al., 2004), using position weight matrices
456 for each TF to compute relative binding scores that reflect *in vitro* binding preferences (Stormo,
457 2013). The exact DNA-binding specificity of PhDEF has not been characterized, but that of its

458 Arabidopsis homologs AP3 and PI has been (Riechmann et al., 1996b). However, since PhDEF
459 DNA-binding specificity might be slightly different to those of AP3 and PI, we decided to predict
460 binding for all MADS-box TFs available in Jaspar 2020, accounting for 23 binding profiles
461 including those of AP3 and PI (Fornes et al., 2020). We hypothesized that sequences predicted to be
462 bound by several MADS-box TFs were putative CArG boxes (the binding site for MADS-box
463 proteins, whose canonical sequence is $CC(A/T)_6GG$, but real binding sites show some variation to
464 this consensus (Aerts et al., 2018)).

465 As a validation of this strategy, we analyzed the genomic sequence of *PhDEF* and found a
466 putative CArG box in the *PhDEF* promoter (visible by the presence of good predicted binding sites
467 for several MADS-box proteins and therefore appearing as a clear black line in Fig. 6C). This CArG
468 box has been validated in the literature: it is highly conserved between distantly-related flowering
469 plants (Rijpkema et al., 2006) and it was shown to be important for *AP3* petal-specific expression
470 and for its auto-activation in Arabidopsis (Hill et al., 1998; Wuest et al., 2012), and for DEF
471 function and binding to its own promoter in Antirrhinum (Schwarz-Sommer et al., 1992). We next
472 applied this predictive approach to the genomic sequences of *AN1* and *AN2*. For *AN1*, we predicted
473 a putative CarG box (*AN1-bs1*) with a very high score for several MADS-box proteins and for AP3
474 and PI in particular, in the terminator region (Fig. 6D). For *AN2*, we also predicted one putative
475 CArG box (*AN2-bs3*), again in the terminator region of the gene (Fig. 6E), although its binding
476 score was more modest in comparison to *AN1-bs1*. The sequence of *AN1-bs1* corresponds to a
477 close-to-canonical CArG box (CTATATTTGG) and the sequence of *AN2-bs3* corresponds to a
478 perfectly symmetrical canonical CArG box (CCATAATAGG).

479 To determine if PhDEF could indeed bind to *AN1-bs1* and *AN2-bs3* and potentially regulate
480 *AN1* and *AN2* expression, we performed gel shift assays using *in vitro* translated PhDEF and/or
481 PhGLO1 proteins (Fig. 6F). We found that, when incubating a 60-bp fragment containing *AN1-bs*1
482 in its center with either PhDEF or PhGLO1, no shift in migration was visible, indicating that neither
483 protein could bind to this site alone. However, when incubating *AN1-bs1* with both PhDEF and
484 PhGLO1 proteins, we observed a clear shift in migration, consistent with the obligate
485 heterodimerization of these proteins necessary for DNA binding (Riechmann et al., 1996a).
486 Similarly, a 60-bp fragment containing *AN2-bs3* in its center, incubated with PhDEF and PhGLO1
487 proteins, resulted in a clear shift in migration. In contrast, a control 60-bp fragment named *AN1-bs2*,
488 located in the *AN1* terminator region but predicted to have a very low binding score (relative score
489 under 0.8 both for AP3 and PI), was not bound by the PhDEF + PhGLO1 protein complex, showing

that our assay was specific. Therefore PhDEF, when dimerized with PhGLO1, is able to bind to sites in putative regulatory regions in *AN1* and *AN2*, suggesting that it might directly regulate the expression of these two genes.

Next, we tested if PhDEF could bind *in vivo* to genomic regions containing *AN1-bs1* and *AN2-bs3* by chromatin immunoprecipitation (ChIP). We produced recombinant PhDEF protein devoid of its highly conserved MADS domain, to avoid cross-reactivity with other MADS-box proteins, and generated a polyclonal antibody against this truncated PhDEF protein. We performed the ChIP assay on second whorl organs (petal or sepal) from wt, *phdef-151* or *phglo1 phglo2* plants at an intermediate stage of development (stage 8). In wt petal samples, we found a significant binding enrichment for some of the genomic fragments (GF) that we tested, and in particular *PhDEF*^{GF1} (Fig. 6G), containing the validated CArG box previously described (Fig. 6C), which is expected since PhDEF activates its own expression.

We also observed a significant binding enrichment in *AN2*^{GF3} (Fig. 6G), containing the previously identified *AN2-bs3* binding site (Fig. 6E). In contrast, no strong enrichment was detected in the *AN1* genomic fragment containing the *AN1-bs1* strong *in vitro* binding site for PhDEF (AN1^{GF3}). Our ChIP assay was specific, since no enrichment was detected for the *phdef-151* mutant, nor for the *phglo1 phglo2* mutant (Fig.6G). The *phglo1 phglo2* samples constitute an indirect control for PhDEF binding, since the PhDEF protein partners PhGLO1/PhGLO2 are absent, thereby indirectly preventing PhDEF binding on DNA. The fact that we do not detect any binding enrichment in these plants shows that our ChIP assay is robust. Therefore, we conclude that PhDEF binds to the terminator region of *AN2 in planta*, and that PhDEF is a putative direct regulator of *AN2* expression in the petal epidermis.

DISCUSSION

In this work, we identified periclinal chimeras expressing the B-class MADS-box gene *PhDEF* in different cell layers of the flower. This layer-specific expression resulted in the correct development of sub-domains of the petal only, showing that epidermal *PhDEF* expression mainly drives limb morphogenesis while its expression in the mesophyll is more important for tube morphogenesis. This indicates that cell layer-specific actions of PhDEF are different and contribute in a complementary fashion to overall petal development.

Contribution of cell layers to mature petunia petals

The SAM of all flowering plants is organized in three independent layers. Generally, it is assumed that L1-derived cells form the epidermis, L2-derived cells produce the mesophyll and sub-epidermal tissue, and L3-derived cells generate the ground tissues (inner mesophyll, vasculature, pith of the stem). However, there is variation to this general pattern between organs; for instance Arabidopsis sepals, stamens and carpels derive from these three layers, while petals derive from the L1 and L2 layers only (Jenik and Irish, 2000). Moreover, the contribution of cell layers can vary between the same organ in different species: for instance, petals from *Datura stramonium* (member of the Solanaceae family like petunia) are derived from all three layers, in contrast to petals from Arabidopsis (Satina and Blakeslee, 1941). Finally, even in one organ from a single species, cell layer contribution is not always homogeneous in different parts of the organ: in *Datura* petals, the L3 only participates in the vasculature at the base of the organ but does not contribute to the distal part of the petal, and the L1 invades the mesophyll at the petal edges (Satina and Blakeslee, 1941).

In fact, the contribution of cell layers to mature organ organization can only be strictly assessed by clonal analysis, where one follows cell lineage using trackable cell-autonomous markers. In petunia, no clonal analysis has been performed so far, hence one can only assume which cell layers participate in petal development based on clonal analyses performed in closely-related species. In *Datura*, periclinal chimeras induced by colchicine treatment and refined histological observations have provided a detailed clonal analysis for cell layers in floral organs (Satina and Blakeslee, 1941). The first visible event of petal initiation is a periclinal cell division from the L2 layer, and further growth of the petal depends primarily on cell divisions from the L2, both anticlinal and periclinal. The L3 layer only contributes to the vascular tissue at the very base of the petal. L1-derived cells form the epidermis by anticlinal divisions, except at the petal edges where periclinal divisions are observed, leading to L1-derived cells invading the mesophyll. Hence, the

Datura petal is formed by all 3 layers with a major contribution of the L1 and L2 layers, and a relative enrichment in L1-derived cells (by thinning of the mesophyll) progressing from the base towards the tip of the petal. In this work, we hypothesized that the petunia petal is formed similarly. Accordingly, we only obtained two phenotypic classes of periclinal chimeras, *star* and *wico*, suggesting that L3-specific *PhDEF* expression probably only leads to a *phdef* mutant phenotype.

The contribution of L1- and L2-derived tissues is heterogeneous in the petunia petal. Indeed, cross-sections in the middle of the petal tube indicate that the mesophyll is thick, with several layers of cells (Fig. 4C). The mesophyll tissue is quite dense in this part of the tube, with lacunae between cells being relatively small. In contrast in the limb, mesophyll cells are very small and interspersed with large lacunae. There is a general thinning of the mesophyll as we progress from the base of the petal towards its edges, whereas the epidermis always appears as a single layer of tightly connected cells. Therefore, the general contribution of cell lineages (L1- or L2-derived) to the petunia petal explains to a large degree the *star* and *wico* phenotypes. Indeed, the limb is mostly derived from the L1 layer, and therefore recovery of this lineage in the *wico* flowers is sufficient to restore limb development. Similarly, the tube is composed of a much higher proportion of mesophyll than epidermis cells, and recovery of the mesophyll lineage in the *star* flowers is sufficient to restore tube development.

Different cell layers drive tube and limb morphogenesis

The *star* and *wico* phenotypes revealed that in petunia petals, the epidermis is the main driver for limb morphogenesis while the mesophyll is the main driver for tube morphogenesis. The epidermis has been proposed to be the layer in control of organ morphogenesis, since it is a layer under tension that restricts growth of the underlying inner tissues that tend to expand (Kutschera and Niklas, 2007). In particular, epidermal expression of the brassinosteroid receptor BRI1 (BRASSINOSTEROID INSENSITIVE 1) is sufficient to restore normal leaf morphogenesis in a *bri1* mutant (Savaldi-Goldstein et al., 2007). Similarly, the expression of the auxin transporter PIN1 (PIN-FORMED 1) in the L1 of the SAM is sufficient to restore normal phyllotaxis in a *pin1* mutant (Kierzkowski et al., 2013). However, pieces of evidence suggest that organ inner layers can have an active role in morphogenesis: for instance, mesophyll-specific expression of *ANGUSTIFOLIA* (*AN*) is sufficient to restore normal leaf width in the Arabidopsis *an* mutant (Bai et al., 2010); leaf shape is controlled by the L2- and L3-derived tissues in *Nicotiana glauca* (McHale and Marcotrigiano, 1998); and the leaf mesophyll is the main player for leaf flatness in Arabidopsis (Zhao et al., 2020).

Moreover, expressing *BRI1* in the root phloem also restores *bri1* plant dwarfism (Graeff et al., 2020). The contribution of cell layers to organ morphogenesis is thus a complex process that varies between organs, species and the genetic systems investigated.

Our work has confirmed that the petunia petal has a modular structure, since tube and limb can develop relatively independently from each other in the *star* and *wico* flowers. This modularity is consistent with previous observations in the literature (described in the Introduction), and in line with the different ecological roles of the tube and the limb for the interaction with pollinators. Our results highlight that a homeotic factor, PhDEF, can participate in the establishment of this modular structure. Indeed, although PhDEF is normally present in all cell layers of the wild-type petal, its action in the different cell layers is mainly responsible for tube or limb development. This provides a possible mechanism, at the tissue level, for the establishment of the modular structure of petunia petals by homeotic genes. It also contributes to the understanding of how homeotic genes can specify at the same time the overall identity of an organ and the coordinated development of its different functional modules.

One may wonder if our findings apply outside of petunia flowers. In snapdragon and Arabidopsis flowers, periclinal chimeras for orthologs of *PhDEF* (*DEF* and *AP3* respectively) or *PhGLO1/PhGLO2* (*GLO* and *PI* respectively) have been previously obtained (Perbal et al., 1996; Vincent et al., 2003; Efremova et al., 2001; Bouhidel and Irish, 1996; Jenik and Irish, 2001; Urbanus et al., 2010b). In snapdragon, expression of *DEF* only in the L1 layer largely restores petal development, particularly in the limb, in contrast to the L2/L3 specific *DEF* or *GLO* expression which causes reduced limb growth (Perbal et al., 1996; Vincent et al., 2003; Efremova et al., 2001). Petals are fused into a tube in snapdragon flowers, but the tube is much more reduced than in petunia, hence conclusions on tube length restoration in the chimeras were not drawn by the authors. However, in light of our results, it is clear that snapdragon chimeras expressing *DEF* or *GLO* in the L2/L3 layers restore tube development to a higher degree than limb development, similar to what we observed. In Arabidopsis that has simple and unfused petals, petal size was never fully restored when *AP3* was expressed in one cell layer only, while petal shape was normal (Jenik and Irish, 2001; Urbanus et al., 2010b); in contrast epidermal expression of *PI* was sufficient to restore normal petal development (Bouhidel and Irish, 1996). Therefore, it seems that the contribution of different cell layers to petal development varies across species and depending on the petal identity gene under investigation.

Autonomous and non-autonomous effects of *PhDEF* expression on petal traits

Our study revealed that petal traits are affected differently by layer-specific *PhDEF* expression (Supplemental Figure S6). For instance, epidermal pigmentation is a clearly autonomous trait, since *star* petals are not pigmented except when wt revertant sectors arise. On the contrary, epidermal cell shape appears to behave as a partially autonomous trait since *star* epidermal cells have an intermediate phenotype between wt petal conical cells and sepal epidermal cells. Finally, organ size and shape are specified non-autonomously in sub-domains of the petal: *PhDEF* expression in the L1 or L2 is sufficient to specify correct shape of the limb or correct size and shape of the tube respectively, suggesting that in these petal domains, layer-specific *PhDEF* expression is sufficient to signal cells from the other layer to grow normally.

The mechanisms for this inter-layer communication remain unknown. Our *in situ* hybridization assays show that the *PhDEF* mRNA is not mobile between layers, but our attempts to detect the PhDEF protein in petal tissue by immuno-histochemistry have been unsuccessful, therefore we do not know if the PhDEF protein itself might be moving between layers, which would be the simplest mechanistic explanation for the non-autonomous traits that we observe. Indeed, in Antirrhinum petals expressing *DEF* in the L2/L3 layers, the DEF protein was found in small amounts in the epidermis and it is likely why petals from these chimeras are faintly pigmented (Perbal et al., 1996; Vincent et al., 2003), This indirectly suggests that no such movement occurs in the *star* petals that are mostly white. In contrast, Arabidopsis AP3 and PI GFP-fusion proteins are unable to move between cell layers, although they can move within the epidermal layer (Urbanus et al., 2010a, 2010b). In any case, even if the PhDEF protein would move between layers in our chimeric flowers, it is likely to be in small amounts only, and possibly at restricted stages of development, otherwise both flower types would have a wt phenotype. Therefore, it is unlikely to be the sole reason for tube and limb correct development in the *star* and *wico* flowers.

Alternatively, the non-autonomous effects that we observed might be triggered by mechanical signals transmitted between layers. For instance, in *star* flowers normal growth of the mesophyll could merely drag along epidermal cells, since cells are connected by their cell walls, which could be sufficient to trigger their expansion and division. Other features, like conical cell shape, might be directly influenced by mechanical signals. Indeed, conical cells are shaped by a circumferential microtubule arrangement controlled by the microtubule-severing protein KATANIN, and altering this arrangement affects conical cell shape (Ren et al., 2017). Microtubule arrangement responds to mechanical signals (Hamant et al., 2008), which are likely to be

transmitted between layers. Therefore, it is possible that the formation of bulging cells in the *star* epidermis is merely triggered by mechanical signals from the growing underlying layer, independent of any petal identity specifier, as was recently evidenced from the observation of conical-like bulges on the hypocotyl of the tubulin kinase mutant *nek6* (Takatani et al., 2020). The molecular or physical nature of the signals involved in communication between layers remains to be explored in full depth.

Towards the gene regulatory networks of petal development

Our *star* and *wico* material granted the opportunity to explore the gene regulatory networks driving petal development in petunia, more specifically by decoupling on the one hand tube vs. limb development, and epidermis vs. mesophyll development on the other. However, these effects are confounded in our dataset, since both epidermis and limb development are affected in *star* flowers, whereas both mesophyll and tube development are affected in *wico* flowers. Further analyses, such as sequencing the transcriptome from *star* and *wico* limb and tube tissues separately, would help uncouple these effects, but it is not easy to clearly separate these different domains during early stages of development, which are crucial stages for petal morphogenesis. Spatial transcriptomics techniques, such as single-cell RNA-Seq, would be ideal to precisely dissect transcriptional changes between layers and domains of the petal at young developmental stages.

Still, we exploited our transcriptomic dataset by focusing our analysis on anthocyanin-related genes, because the molecular link between the early establishment of petal identity by homeotic transcription factors, such as PhDEF, and the late establishment of petal maturation traits, such as anthocyanin accumulation, was unknown. For this, we examined the presence of anthocyanin-related genes among genes downregulated both in *star* and *phdef-151* samples, but not differentially expressed in *wico* samples. We found a very strong enrichment of anthocyanin-related genes in this dataset, suggesting that the initial triggering event for most of the anthocyanin biosynthesis pathway was missing in *star* flowers.

Finally, we investigated the direct link between PhDEF and petal pigmentation and found that, *in vitro*, the PhDEF + PhGLO1 protein complex directly binds to predicted binding sites in the regulatory regions of *AN1* and *AN2*. We confirmed that PhDEF binds to the corresponding genomic region of *AN2 in plant*a by ChIP, but not for *AN1*, confirming that *in vitro* binding does not necessarily imply *in vivo* binding, the last being strongly influenced by the local chromatin landscape. The binding site of PhDEF that we identified on *AN2* (*AN2-bs3*) lies in the terminator

region of the gene (and the next gene on the chromosome is more than 100 kb away), which was surprising since around 80 % of MADS binding sites are located within the 3 kb promoter region of their target genes (Aerts et al., 2018). However, the presence of a binding site in the terminator region is still compatible with an activating role in transcription, through DNA looping to the promoter (Jash et al., 2012) or by promoting transcription termination and reinitiation (Wang et al., 2000). Other putative CArG boxes in the genomic region of *AN2* are *AN2-bs1*, located 866 bp upstream the ATG in the promoter region, and *AN2-bs2*, located 62 bp downstream the STOP codon in the 3'UTR region. Both have non-canonical CArG box sequences (GAAAAGTAG for *AN2-bs1* and TCTTTTTTAA for *AN2-bs2*) and were not bound in our gel shift assay (Supplemental Figure S8). Still, it is possible that regulators other than MADS-box TFs could form protein complexes with PhDEF and mediate looping to the promoter region of *AN2*. The precise mechanism by which PhDEF might activate *AN2* transcription remains to be uncovered.

When aligning Petunia *AN2* sequences, we found that *AN2-bs3* lies in a globally non-conserved region of the gene (Supplemental Figure S8), and *AN2-bs3* is only conserved in *Petunia inflata*, one of the likely original parents of *Petunia x hybrida* (Bombarely et al., 2016). However, *cis*-regulatory elements are very fluid and their sequences can change rapidly in short evolutionary times, without the gene regulation being necessarily lost (see for instance (Schmidt et al., 2010; Krieger et al., 2022)). Moreover, petal pigmentation is an extremely labile trait, and even within the *Petunia* genus it has been lost and regained at least two times independently (Quattrocchio et al., 1999; Esfeld et al., 2018; Berardi et al., 2021). Therefore, the fact that *AN2-bs3* is not largely conserved does not necessarily imply that it is an unimportant site for *AN2* regulation in *P. hybrida*.

The fact that we detected strong *in planta* binding of PhDEF to *AN2*, together with the fact that *AN2* expression is strongly down-regulated in the *phdef-151* transcriptome, suggests that PhDEF is a good candidate to directly activate *AN2* expression in the petal. Ectopic expression of *AN2* in petunia leaves is sufficient to trigger anthocyanin accumulation in this tissue, by inducing *AN1* expression among others (Spelt et al., 2000; Quattrocchio et al., 1998). Therefore, if PhDEF indeed activates *AN2* expression, it should be sufficient to launch the whole pigmentation pathway in the wt petal limb. However, to fully support this conclusion, functional tests on the role of PhDEF binding to *AN2-bs3* in regulating *AN2* expression should be conducted. A direct link between petal identity and pigmentation has yet to be established, although genetic evidence in orchid flowers strongly implied that different B-class proteins heteromeric complexes are responsible for specific pigmentation spots in the different petal types, but physical binding of these

B-class protein complexes on pigmentation genes was not tested (Hsu et al., 2021). The direct target genes of B-class proteins have been identified by ChIP-Seq and transcriptomic analyses in Arabidopsis (Wuest et al., 2012), but this species has unpigmented petals, thereby preventing us to draw any possible link between petal identity and pigmentation. The petunia petal is the ideal system to test this direct link, and our results suggest that PhDEF might be the direct link between petal identity and its epidermal pigmentation.

MATERIALS AND METHODS

Plant materials, growth conditions and plant phenotyping

The *phdef-151* plants were obtained from the *Petunia x hybrida* W138 line and were grown in a culture room in long day conditions (16h light 22°C; 8h dark 18°C; 75-WValoya NS12 LED bars; light intensity: 130 µmol m^{-2} s^{-1}). Hundreds of *phdef-151* flowers were observed over several years, and all of them show the same phenotype, also identical to the *def-1* and *green petal (gp)* mutant flowers (de Vlaming et al., 1984; van der Krol et al., 1993). The *wico* and *star* flowers were repeatedly obtained from several different *phdef-151* individuals and were maintained by cuttings. For this, branches where several *star* or *wico* flowers were already visible were cut into a ca. 5-cm long segment, large flowers and leaves were removed and the branch segment was planted into an hydrated Jiffy peat soil pellet (Jiffy Products International AS, Norway). When roots became visible on the outside of the pellet, it was transferred into soil. Plant and flower pictures were obtained with a CANON EOS 450D camera equipped with objectives SIGMA 18-50mm or SIGMA 50mm. To measure tube length, the flower was cut longitudinally and photographed from the side. To measure limb area, the limbs were flattened as much as possible on a glass slide covered with transparent tape and photographed from the top. The photographs were used to measure D1 and D2 lengths and limb area with ImageJ.

Genotyping

Extraction of genomic DNA from young leaf tissue was performed according to (Edwards et al., 1991). The region spanning the *dTph1* insertion site in *PhDEF* was amplified using primers MLY0935/MLY0936 (Supplemental Table S2). PCR products were separated on a 2% (w/v) agarose gel, fragments of interest were purified using the NucleoSpin® Gel and PCR Clean-up kit (Macherey-Nagel), and sequenced with Eurofins SupremeRun reactions.

In situ RNA hybridization

Floral buds from wt, 2 *wico* and 1 *star* lines were fixed overnight in FAA (3.7% (v/v) formaldehyde, 5% (v/v) acetic acid, 50% (v/v) ethanol), cleared in Histo-clear and embedded in paraffin to perform 8 µm sections. *PhDEF* cDNA sequence was amplified from wt petunia inflorescence cDNAs with primers MLY1738/MLY1739 (Supplementary Table 2), generating a 507 bp fragment excluding the part encoding the highly conserved DNA-binding domain. The digoxigenin-labeled RNA probe was synthesized from the PCR fragment by *in vitro* transcription, using T7 RNA polymerase (Boehringer Mannheim). RNA transcripts were hydrolyzed partially for 42 min by incubation at 60°C in 0.1 M Na_2CO_3/$NaHCO_3$ buffer, pH 10.2. Later steps were performed as

described by (Cañas et al., 1994). For imaging, slides were mounted in Entellan (Sigma) and imaged with a Zeiss Axio Imager M2 light microscope equipped with a Zeiss Axio Cam HRc camera.

Petal cross-sections

Small pieces (around 5 mm^2) of tissue were harvested from the proximal and distal parts of wt mature sepals, and from the tube and limbs of wt, *star* and *wico* mature petals. Samples were fixed overnight in FAA (3.7% (v/v) formaldehyde, 5% (v/v) acetic acid, 50% (v/v) ethanol) and dehydrated in an ethanol series. Preinfiltration was performed in a 1:1 mixture of ethanol:Technovit 7100 (Electron Microscopy Sciences) for 4 h under light agitation, then overnight in a 1:3 ethanol:Technovit 7100 mixture. Infiltration was performed in the infiltration solution for 1.5 h under vacuum, then for one night followed by one additional week. Samples were arranged in the moulds with the polymerization solution for 2 h at room temperature, then mounted with the Technovit 3040 resin to relieve the blocks from the moulds. Blocks were sectioned with a microtome to generate 3-7 µm-thick sections. Slides were incubated for 10 minutes in a 0.1% (w/v) toluidine blue solution and imaged with a Zeiss Axio Imager M2 light microscope equipped with a Zeiss Axio Cam HRc camera.

Scanning electron microscopy (SEM)

Scanning electron micrographs were obtained with a HIROX SH-1500 bench top environmental scanning electron microscope equipped with a cooling stage. Samples were collected and quickly imaged to limit dehydration, at -5°C and 5 kV settings. For cell area and length measurements, pictures were taken from 3 petal tubes and 3 petal limbs from different wt, *star* and *wico* flowers. For each sample, 3 pictures were taken and 5 cells (for the tube) or 10 cells (for the limb) were measured for each picture. Measures were performed with ImageJ by manually drawing the outline or length of the cells.

RNA-Seq

Petal tissue was collected at 1 pm from several plants stemming from a single *star* line, a single *wico* line, and several individual wt plants (progeny of a single *star* flower) and *phdef-151* plants (progeny of the same *star* flower). Tube length was macroscopically measured to compare stages, the corolla was cut open and stamens were removed as much as possible from the corolla by pulling on the filaments fused to the tube. One biological replicate contains total petal tissue from 2 flowers. Tissue was ground in liquid nitrogen and RNA was extracted with the Spectrum Plant Total RNA Kit (Sigma) including on-column DNase digestion (Sigma). RNA integrity and quantity were

774 determined by a Bioanalyzer RNA 6000 Nano assay (Agilent). Libraries were prepared with poly-A
775 enrichment and single-end 75-bp sequencing was performed on a NextSeq 500 platform (Illumina).
776 16 to 23 million reads were recovered per library. Reads were checked for quality with FastQC
777 v0.11.4 (https://www.bioinformatics.babraham.ac.uk/projects/fastqc/), adaptors and low-quality
778 ends were trimmed with Cutadapt v 1.16 (Martin, 2011) and custom Perl scripts. The reference
779 genome sequence used for transcriptome analysis is the *Petunia axillaris* v1.6.2 HiC genome
780 published in (Bombarely et al., 2016) and further scaffolded by HiC by DNAzoo (Dudchenko et al.,
781 2017, 2018); gene annotations were transferred from the published assembly to the HiC-scaffolded
782 version using Blat (Kent, 2002), Exonerate (Slater and Birney, 2005) and custom Perl scripts. In the
783 rare cases when gene annotations from the published genome mapped to several regions in the HiC-
784 scaffolded genome, these different putative genes were identified by a letter added at the end of the
785 gene identifier (for instance Peaxi162Scf00179g00121a). The complete set of reads was mapped on
786 the reference genome sequence using HISAT2 v2.2.1 (Kim et al., 2015) to identify splicing sites,
787 before performing mapping sample per sample. Reads per gene were counted using FeatureCounts
788 v1.5.1 (Liao et al., 2014). DESeq2 version 3.12 (Love et al., 2014) was used with R version 4.0.3 to
789 perform the Principal Component Analysis and the differential gene expression analysis. Genes
790 having less than 10 reads in the sum of all samples were considered as non-expressed and
791 discarded. Genes were considered to be differentially expressed if log2FoldChange > 1 or < -1, and
792 p-adjusted value < 0.01. The bioinformatic pipeline for annotation transfer, read cleaning, splicing
793 site discovery, read mapping and preliminary DESEq2 results can be found at gitbio.ens-
794 lyon.fr/rdp/petunia_star_wico_rnaseq. Venn diagrams were built with InteractiVenn (Heberle et al.,
795 2015). Due to the automatic gene name annotation pipeline used in (Bombarely et al., 2016) based
796 on homology with tomato (*Solanum lycopersicum*) proteins, many of the previously characterized
797 petunia genes have not been annotated according to their first described name, making
798 interpretation of some of the RNA-Seq results less straightforward. We have manually added
799 annotations of 42 genes from the anthocyanin biosynthesis pathway based on the Supplementary
800 Note 7 from (Bombarely et al., 2016), and 31 type-II MIKC-C MADS-box genes based on previous
801 studies from the literature ; these annotations can be found in the Supplemental Dataset S1 of this
802 manuscript. We noticed that the gene annotations from three major pigmentation genes, *DFR*
803 *(DIHYDROFLAVONOL-4-REDUCTASE,* Peaxi162Scf00366g00630), *CHSa* (*CHALCONE*
804 *SYNTHASE a*, Peaxi162Scf00047g01225) and *PH1* (Peaxi162Scf00569g00024) were lost during
805 the gene annotation transfer procedure, because they lie in regions of the genome that are still

poorly resolved. Therefore, we manually searched the position of these transcripts in the HISAT2 output and we were able to map part of the *DFR* and *CHSa* genes to two small scaffolds, while *PH1* position was not found. We added the transcript positions of *DFR* and *CHSa* in the gtf/gff files before running FeatureCounts. The read counts for *DFR* and *CHSa* reported in Supplemental Figure S7 are therefore an under-estimation of their actual expression levels, since we miss part of the genes.

Prediction of MADS-box TF binding sites

Genomic sequences from *AN1*, *AN2* and *PhDEF* from the *Petunia x hybrid*a R27 line, starting 3 kb upstream the START codon and ending 1 kb downstream the STOP codon, were scanned with all MADS-box TF matrices included in the Jaspar 2020 database (http://jaspar.genereg.net), only removing matrices from AGL42 and AGL55 which are much shorter than the other matrices and therefore yield much higher scores. Relative scores above 0.86 were plotted against their genomic position.

Electrophoretic mobility shift assays (EMSAs)

CDS sequences from *PhDEF* and *PhGLO1* were amplified from *Petunia x hybrida* R27 inflorescence cDNAs with primers MLY2382/MLY2383 and MLY2384/2385 respectively (Supplemental Table S2) and cloned into the *in vitro* translation vector pSPUTK (Stratagene) by NcoI/XbaI restriction. From these vectors, the PhDEF and PhGLO1 proteins were produced with the TnT SP6 High-Yield Wheat Germ Protein Expression System (Promega) according to the manufacturer's instructions. The terminator regions from *AN1* (0.8 kb) and *AN2* (1 kb), and part of the promoter region of *AN2* (1.2 kb), were amplified from *Petunia x hybrida* R27 genomic DNA with primers from Supplemental Table S2 and cloned into pCR-BluntII-TOPO (ThermoFisher). Binding sites were amplified from these plasmids with primers listed in Supplemental Table 2, with the forward primer labelled with Cy5 in 5'. The labelled DNA was purified and incubated with the TnT *in vitro* translation mixture as described in (Silva et al., 2015) before loading on a native acrylamide gel.

PhDEF protein and antibody production

The *PhDEF* truncated cDNA (without the sequence coding for the MADS domain) was chemically-synthesized with optimization for expression in *Escherichia coli* and cloned into a pT7 expression vector by Proteogenix (www.proteogenix.science). The expected PhDEF protein starts at amino acid 60 (PSITT...) and ends at the last amino acid of the sequence (...FALLE), and a 6xHis tag was added at the N-terminal part of the protein. The 6xHis-PhDEF protein was purified by affinity

838 column with a Nickel resin under denaturing conditions (8M urea) by Proteogenix. The purified
839 protein was injected in two rabbits for immunization by Proteogenix, to generate PhDEF-directed
840 polyclonal antibodies, that were purified by affinity against the antigen. Both lots of purified
841 antibodies were validated by immunoblot in petal or sepal tissues from wt, *phdef-151* and *phtm6*
842 samples.

843 **Chromatin immunoprecipitation (ChIP)**

844 One biological replicate comprises the full corolla from 2 flowers (wt), second whorl sepals from 3
845 flowers (*phdef-151*) or second whorl sepals from 3 to 4 flowers (*phglo1 phglo2*), and the full
846 experiment was performed for 3 biological replicates for wt and *phdef-151* and 2 biological
847 replicates for *phglo1 phglo2*. Samples at stage 8 were collected and ground in liquid nitrogen.
848 Ground tissue was resuspended into 10 mL fixation buffer (10 mM Hepes pH7.6, 0.5 M sucrose, 5
849 mM KCl, 5 mM $MgCl_2$, 5 mM EDTA pH8, Complete Protease Inhibitor Cocktail (Merck), 14 mM
850 2-mercaptoethanol) and a double cross-linking was performed at room temperature (1 hour with
851 disuccinimidyl glutarate at 2.5 mM with gentle shaking, and 5 minutes with formaldehyde 1%
852 (v/v)). Cross-linking was stopped by adding glycine at 200 mM and samples were put directly on
853 ice. Cells were lysed with a 40 mL-Dounce tissue grinder (Duran Wheaton Kimble), Triton X-100
854 was added at 0.6% (w/v) and the lysate was filtered subsequently through 100 µm and 40 µm nylon
855 meshes to recover nuclei. Nuclei were pelleted for 10 minutes at 3,000 g at 4°C, and the pellet was
856 resuspended in 300 µL of cold nuclear isolation buffer (i.e. fixation buffer without 2-
857 mercaptoethanol), carefully deposited on 600 µL of a 15% Percoll solution (15 % (v/v) Percoll, 10
858 mM Hepes pH8, 0.5 M sucrose, 5 mM KCl, 5 mM $MgCl_2$, 5 mM EDTA pH8) and centrifuged for 5
859 minutes at 2,000 g at 4°C. The pellet was resuspended into 900 µL of cold nuclear lysis buffer (50
860 mM Tris-HCl pH7.5, 0.1% (w/v) SDS, 10 mM EDTA pH8) to lyse the nuclei, and chromatin was
861 sonicated twice for 15 minutes with a Covaris S220 sonicator (peak power 105, Duty factor 5,
862 Cycles/Burst 200 for 900s). For each sample, 25 µL of magnetic protein-A Dynabeads and 25 µL of
863 magnetic protein-G Dynabeads (Invitrogen) were washed twice with 100 µL of cold ChIP dilution
864 buffer (15 mM Tris-HCl pH7.5, 150 mM NaCl, 1% (w/v) Triton X-100, 1 mM EDTA pH8) using a
865 magnetic rack (MagRack 6, Cytiva). Beads were mixed with 2.5 µg of anti-PhDEF antibody and 1.8
866 mL of cold ChIP dilution buffer, and incubated for 2 hours at 4°C on a rotating wheel. Sonicated
867 chromatin was centrifuged for 5 minutes at 15,000 g at 15°C, and 25 µL of supernatant (for wt
868 samples) or 50 µL of supernatant (for *phdef-151* and *phglo1 phglo2* samples) was added to the mix
869 of beads and antibody, and incubated overnight at 4°C on a rotating wheel. Beads were washed

twice (one quick wash and one long wash with 15 minutes incubation on a rotating wheel) with each of the following buffers: low salt wash buffer (0.1% (w/v) SDS, 1% (w/v) Triton X-100, 2 mM EDTA pH8, 20 mM Tris-HCl pH8, 150 mM NaCl), high salt wash buffer (0.1% (w/v) SDS, 1% (w/v) Triton X-100, 2 mM EDTA pH8, 20 mM Tris-HCl pH8, 500 mM NaCl), LiCl wash buffer (0.25 M LiCl, 1% (v/v) NP40/Igepal,1% (w/v) deoxycholate, 1 mM EDTA pH8, 20 mM Tris-HCl pH8) and TE buffer. Elution was performed twice with 250 µL of elution buffer (0.1 M $NaHCO_3$, 1% (w/v) SDS) at 65°C. IP and input samples were decrosslinked overnight at 65°C by adding NaCl at 200 mM, then incubating for 2 h at 42°C with 20 µg proteinase K in 10 mM EDTA pH8 and 40 mM Tris-HCl pH6.5. DNA was purified with phenol:chloroform:isoamyl alcohol (25:24:1) followed by chloroform:isoamyl alcohol (24:1), precipitated with ethanol at -20°C and the pellet was washed with ethanol 70 %. The dry pellet was recovered in 50 µL TE and 1 µL was used for each qPCR reaction, which was performed in technical triplicates for each biological replicate (3 for wt and *phdef-151*, 2 for *phglo1 phglo2* and the control without antibody). The qPCR reaction was performed with 1X FastStart Universal SYBR Green (Merck) and 0.3 µM primer mix (Supplemental Table S2), for 40 cycles (15 seconds at 95°C, 1 minute at 60°C) in a QuantStudio 6 Flex instrument (ThermoFisher). Percentage of input (enrichment) was calculated as 100* e^(CtIN – log2(DF) – CtIP), with e the efficiency of the primer pair, CtIN the average Ct value for the Input sample, DF the dilution factor and CtIP the average Ct value for the IP sample), as described in (Solomon et al., 2021). The significance of the enrichment was evaluated with a one-tailed t-test comparing the enrichment of the test region to the average of the enrichments of the two negative regions.

Sequence alignments

The genomic sequences (3 kb upstream of the transcription starting site, 1 kb downstream of the STOP codon) of *AN2* from Solanaceae species were retrieved by blasting the *P. hybrida AN2* coding sequence against genomic sequence resources: *AN2* sequences from *Nicotiana tabacum* (K326) (Sierro et al., 2014), *Petunia axillaris* and *Petunia inflata* (Bombarely et al., 2016) were retrieved from the Sol Genomics Network website (solgenomics.net); *AN2* sequence from *Petunia exserta* was retrieved from DNA Zoo (https://www.dnazoo.org/assemblies/Petunia_exserta); *AN2* sequence from *Petunia secreta* was retrieved from NCBI GenBank, BioProject PRJNA674325. *AN2* genomic sequences were aligned using mVista (Mayor et al., 2000) with *P. hybrida AN2* as reference, with the AVID algorithm. Detailed alignment of the *AN2-bs3* region was performed with KAlign (Lassmann, 2019) and visualized with MView (Madeira et al., 2022).

902
903 **Statistical analysis**
904 RStudio was used for statistical analysis of the numerical data. To test for differences in mean
905 values between samples, a Shapiro-Wilk test was performed to test for normal distribution of the
906 data, and accordingly to the results, either a Student's t-test or a Wilcoxon rank sum test was
907 applied. To test for differences between expected and observed frequencies, a Chi-square test or a
908 Fisher's exact test (for small samples) was applied. Details about the conditions used for the tests
909 are given in the corresponding Figure or Table legends, and all statistical test results are reported in
910 Supplemental Data Set S3.
911
912 **ACCESSION NUMBERS**
913 Sequence data from this article can be found in the EMBL/GenBank data libraries under accession
914 numbers OQ418981 (*AN1*), OQ418982 (*AN2*) and OQ418983 (*PhDEF*). Raw sequence reads for
915 the wt, *phdef-151*, *star* and *wico* second whorl organs transcriptome have been deposited in
916 BioProject with the accession number PRJNA951505.
917 **SUPPLEMENTAL DATA**
918 **Supplemental Figure S1.** Additional pictures of *star* and *wico* flowers.
919 **Supplemental Figure S2.** Stamens are unfused to the tube in *wico* flowers.
920 **Supplemental Figure S3.** Additional pictures of *PhDEF* transcript *in situ* hybridization in wild-
921 type, *star* and *wico* flowers.
922 **Supplemental Figure S4.** Wild-type and pink wild-type flowers observed in the progeny of a *star*
923 parent.
924 **Supplemental Figure S5.** Epidermal revertant sectors on *star* petals.
925 **Supplemental Figure S6.** Autonomous and non-autonomous effects in *star* and *wico* petals.
926 **Supplemental Figure S7.** Expression of B-class genes and a subset of pigmentation genes in wild-
927 type, *star*, *wico* and *phdef-151* samples.
928 **Supplemental Figure S8.** Additional information on putative PhDEF binding sites on the *AN2*
929 genomic sequence.
930
931 **Supplemental Table S1. Genotyping results of the progeny of a *star* flower.**
932 **Supplemental Table S2.** List of primers used in this study.
933

Supplemental Dataset S1. Differential gene expression calculated by DESeq2.

Supplemental Dataset S2. List of the 451 genes downregulated in *star* and *phdef-151* samples, and not differentially expressed in *wico* samples.

Supplemental Dataset S3. Summary of statistical analyses.

FUNDING INFORMATION

This work was supported by a PhD fellowship to M.C. from the French Ministry of Higher Education and Research, by a grant to Q.C.S. and M.M. from the Agence Nationale de la Recherche (grant ANR-19-CE13-0019, FLOWER LAYER), by a grant to M.M. from IDEXLYON (Université de Lyon, grant ELAN-ERC), and by a grant to V.H. and C.Z. from the Agence Nationale de la Recherche (grant ANR-16-CE92-0023, FLOPINET).

ACKNOWLEDGMENTS

We thank Patrice Bolland, Justin Berger and Alexis Lacroix for plant care assistance, the PLATIM platform (SFR BioSciences Lyon, UAR3444/CNRS, US8/Inserm, ENS de Lyon, UCBL) for electron microscopy technical support, Benjamin Gillet and Sandrine Hugues from the sequencing platform of the Institut de Génomique Fonctionnelle de Lyon for library preparation and sequencing of the transcriptomes of this study, Rémy Belois for assistance for *in situ* hybridization experiments and Daniel Bouyer and Nicolas Dalle for assistance for chromatin immunoprecipitation experiments. We gratefully acknowledge support from the PSMN (Pôle Scientifique de Modélisation Numérique) of the ENS de Lyon for the computing resources.

AUTHOR CONTRIBUTIONS

M.M. and M.V. conceived and designed the experiments. M.C., Q.C.S., P.M., P.C., V.H. and S.R.B. performed the experiments. M.C., Q.C.S., J.J., M.V. and M.M. analyzed the data. M.C., C.Z., M.V. and M.M. wrote the article.

960 **TABLES**

961 **Table 1.** Progeny of the *star* and *wico* flowers after selfing.

962 7 *wico* flowers and 4 *star* flowers have been selfed and their progeny has been phenotyped and
963 classified into *phdef*, wt or pink wt phenotype. Summing the *star* progeny for the 4 parents gives 25
964 *phdef*, 16 wt and 39 pink wt plants, which is not significantly different to a 1:1:2 ratio (chi-square
965 test, p = 0.35). * For *wico*, we found 4 plants with wt or pink wt flowers in the progeny, and all of
966 them were linked to the presence of a *de novo* transposon excision from the *PhDEF* locus, restoring
967 either a *PhDEF+6* (in the case of pink wt progeny) or a wild-type *PhDEF* (in the case of the wt
968 progeny) allele.

969

		Phenotype of the progeny (% of the total)		
		phdef	wt	pink wt
Parent flower	*wico*-1	15 (94%)		1 (6%) *
	wico-2	14 (88%)	1 (6%) *	1 (6%) *
	wico-3	16 (100%)		
	wico-4	15 (94%)		1 (6%) *
	wico-5	16 (100%)		
	wico-6	12 (100%)		
	wico-7	12 (100%)		
	star-1	11 (46%)	4 (17%)	9 (38%)
	star-2	4 (25%)	4 (25%)	8 (50%)
	star-3	7 (29%)	5 (21%)	12 (50%)
	star-4	3 (19%)	3 (19%)	10 (63%)

970

971

972

973

974

FIGURE LEGENDS

Figure 1. Macroscopic description of the *star* and *wico* flowers.

(A) *phdef-151* mutant plant harboring one branch with *wico* revertant flowers and one branch with *star* revertant flowers. Scale bar: 1 cm. **(B-I)** Representative wild-type (wt) (B), *phdef-151* (C), *star* (D-F) and *wico* (G-I) flowers from a top (left) and side (right) view. The *star* and *wico* flowers come from independent reversion events (from different *phdef-151* plants or from different branches of a single *phdef-151* plant). Scale bar: 1 cm. **(J)** Two *star* flowers with additional L1-revertant sectors in one petal (left) or one petal and two half petals (right). Scale bar: 1 cm. **(K)** Schematic cross-section of a wt flower, showing stamens (in green) partially fused to the petal tube. The region of the tube fused to stamens is named D1, and the region of the tube where stamens are free is named D2, as defined in (Stuurman et al., 2004). **(L)** Average length of regions D1, D2 and total tube length in wt, *star* and *wico* flowers. **(M)** Average limb area in wt, *star* and *wico* flowers. **(N)** Average ratio between limb area and tube length in wt, *star* and *wico* flowers. n = 7 wt flowers, n = 12 *star* flowers from 4 different branches, n = 18 *wico* flowers from 5 different branches. Student's t test, two-sided with Welch correction for D1, D2 and tube length, two-sided without Welch correction for limb area and limb area/tube length ratio (* $p < 0.05$, ** $p < 0.01$, *** $p < 0.005$). Error bars represent ± s.e.m.

Figure 2. Sequencing the *PhDEF* excision alleles in *star* and *wico* flowers.

(A) *PhDEF* gene model indicating the position of the *dTph1* insertion in the first exon (black triangle) and the primers used for subsequent amplification and sequencing (in red). **(B)** Amplicons generated with primers spanning the *dTph1* insertion site, on genomic DNA from *phdef-151* second whorl organs and *star* and *wico* sepals and petals. The large fragment still contains the *dTph1* transposon inserted (expected size: 407 bp), while small fragments result from different events of *dTph1* excision (expected size: 115 bp) and were subsequently sequenced. **(C)** The small *PhDEF* fragments from (B) were sequenced in the second whorl organs of flowers with a *phdef* (n = 2), *star* (n = 14) and *wico* (n = 14) phenotype. The nucleotidic sequence and predicted protein sequence are indicated, with stop codons represented by a *star*. Additional nucleotides or amino-acids as compared to the wt sequences are indicated in red. n = number of independent reversion events where the same excision footprint was found. wt = wild-type.

Figure 3. Localization of the *PhDEF* transcript in wt, *star* and *wico* flowers by *in situ* hybridization.

Longitudinal sections of wild-type (wt) (A, B, C), *star* (D, E, F) and *wico* (G, H, I) flowers or young petals hybridized with a digoxigenin-labelled *PhDEF* antisense probe. At the earliest stage chosen (A, D, G), sepals are initiating and *PhDEF* is expressed in the future petal / stamen initiation domain. Note that if the section was not performed at the center of the flower, the *PhDEF* signal might artificially appear to be in the middle of the flower (as in D) whereas it is actually on its flanks. At the middle stage chosen (B, E, H), stamens (white arrowhead) and petals (red arrowhead) are initiating, and *PhDEF* is expressed in both primordia. The meristematic L1, L2 and L3 layers are indicated on the wt sections (A, B). *PhDEF* expression is also detected at the tip of young petal limb (C, F, I). The epidermis and mesophyll layers, derived from the previous L1 and L2 meristematic layers, are indicated on the wt section (C). se: sepals. Scale bar: 50 µm.

Figure 4. Epidermal and mesophyll cell identities in wt petals and sepals, and *star* and *wico* petals.

(A) From left to right: wild-type (wt) petals, wt sepals, *star* petals and *wico* petals cut open longitudinally to show areas used for scanning electron microscopy and cross-sections. Petals were subdivided into limb and tube area, and sepals were subdivided into a distal and a proximal part, as shown by the dotted white rectangles. Scale bar: 1 cm. **(B)** Representative scanning electron micrographs from the adaxial side of a wt petal, wt sepal, *star* petal and *wico* petal (from left to right). The red arrowhead points to a stomata and the white arrowhead points to a trichome. Scale bar: 30 µm. **(C)** Representative cross-sections from wt petals, wt sepals, *star* petals and *wico* petals (from left to right) stained with toluidine blue. The adaxial and abaxial epidermis and the mesophyll are indicated on the wt petal sections. Scale bar: 100 µm. **(D)** Average limb cell area from the adaxial side of wt, *star* and *wico* petals (n = 30 cells). Student's t test with Welch correction, two-sided (* $p < 0.05$, ** $p < 0.01$, *** $p < 0.005$). Error bars represent ± s.e.m. **(E)** Average tube cell length from the adaxial side of wt, *star* and *wico* petals (n = 40 cells for wt, 45 cells for *star* and *wico*). Wilcoxon rank sum test, two-sided (* $p < 0.05$, ** $p < 0.01$, *** $p < 0.005$). Error bars represent ± s.e.m. **(F)** Limb area from wt (top) and *wico* (bottom) petals, after their adaxial epidermis was manually peeled. For wt, the upper half of the picture shows the white underlying mesophyll. For *wico*, the green triangular area shows the green (chloroplastic) underlying mesophyll. Scale bar: 300 µm.

Figure 5. Gene differential expression in *star* and *wico* petals.

(A) Flowers from wild-type (wt), *star*, *wico* and *phdef-151* at stages 4, 8 and 12 (only stage 12 for *phdef-151*), whose petals or sepals were harvested for transcriptome sequencing. Flowers at anthesis are shown for comparison. Scale bar: 1 cm. **(B)** Principal Component Analysis plot of the samples after analysis of variance with DESeq2, showing that the first principal component corresponds to the developmental stage and the second principal component corresponds to the genotype. **(C)** Number of upregulated and downregulated genes in *star*, *wico* and *phdef-151*, as compared to wt at the corresponding stages. **(D)** Venn diagram recapitulating the number of differentially expressed genes (DEGs) in *star*, *wico* and *phdef-151* petal samples at stage 12, as compared to wt, and their different intersections. Each sector contains the number of DEGs, and between parenthesis is the percentage of genes that it represents from the total number of DEGs in the corresponding sample, with a colour code (red = percentage of DEGs from *star* samples / blue = from *wico* samples / black = from *phdef-151* samples).

Figure 6. PhDEF binds to *AN2* regulatory region *in vitro* and *in vivo*.

(A, B) Expression (as normalized read counts calculated by DESeq2) of *AN1* (A) and *AN2* (B) in wild-type (wt), *star*, *wico* and *phdef-151* second whorl organs at stages 4, 8 or 12. Stars indicate significant down-regulation (log2FC < -1 and adjusted p-value < 0.01). **(C-E)** Relative score profiles for AP3 (red diamond), PI (blue triangle) and all other MADS-box transcription factors (black dots) available on Jaspar, on the genomic sequences of *PhDEF* (C), *AN1* (D) and *AN2* (E). The relative score is computed using the position weight matrix of each transcription factor and is between 0 and 1; only relative scores higher than 0.86 are shown here. The gene model is represented above the score profile with exons as grey rectangles, the transcription start site as an arrow, and the gene model is aligned with the position of the predicted binding sites (bs). For *PhDEF*, the position of a putative CArG box, as explained in the main text, is indicated by a red arrow. The positions of the sites tested by gel shift in panel F and Supplemental Figure S8 are indicated: putative PhDEF binding sites (*AN1-bs1, AN2-bs1, AN2-bs2* and *AN2-bs3*) and a negative control with a low predicted binding score (*AN1-bs2)*. Sites indicated in red were bound in the gel shift assay, while sites indicated in grey were not bound. In orange, are depicted the genomic fragments (GF) tested by chromatin immunoprecipitation in (G). **(F)** Representative electrophoretic mobility shift assay (EMSA) gel performed with a combination of *in vitro*-translated PhDEF and/or

PhGLO1 proteins, and Cy5-labelled *AN1-bs1, AN1-bs2* or *AN2-bs3* DNA fragments, whose position is depicted in (C-E). Similar results were obtained in 5 additional independent assays for *AN1-bs1*, 2 additional independent assays for *AN2-bs3* and 4 additional independent assays for *AN1-bs2*. **(G)** Enrichment (as percentage of INPUT) of binding of PhDEF to different genomic regions of the chromatin purified from wt, *phdef-151* or *phglo1 phglo2* second whorl organs at stage 8, after immunoprecipitation with an anti-PhDEF directed antibody. The control without antibody was performed on chromatin isolated from wt petals. The position of the genomic fragments tested is depicted in (C-E). Neg1 and Neg2 represent two negative control fragments located in the promoter region of genes not differentially expressed in the *phdef-151* mutant, and present on different chromosomes than *PhDEF*, *AN1* and *AN2*. For unknown reasons, the Neg1 control region could never be amplified in the *phglo1 phglo2* samples. *Star*s indicate a significant enrichment of test regions over the average of the two negative control regions for each chromatin sample (one-sided t-test with Welch correction, * $p<0.05$, ** $p<0.005$; n = 3 biological replicates for wt and *phdef-151*, 2 biological replicates for *phglo1 phglo2* and the control without antibody). Error bars represent ± s.e.m.

1085 **REFERENCES**

1086

Abe, M., Takahashi, T., and Komeda, Y. (1999). Cloning and characterization of an L1 layer-specific gene in Arabidopsis thaliana. Plant Cell Physiol **40**: 571–580.

Aerts, N., de Bruijn, S., van Mourik, H., Angenent, G.C., and van Dijk, A.D.J. (2018). Comparative analysis of binding patterns of MADS-domain proteins in Arabidopsis thaliana. BMC Plant Biol **18**: 1–16.

Albert, N.W., Lewis, D.H., Zhang, H., Schwinn, K.E., Jameson, P.E., and Davies, K.M. (2011). Members of an R2R3-MYB transcription factor family in Petunia are developmentally and environmentally regulated to control complex floral and vegetative pigmentation patterning. Plant J **65**: 771–784.

Angenent, G.C., Busscher, M., Franken, J., Mol, J.N., and van Tunen, A.J. (1992). Differential expression of two MADS box genes in wild-type and mutant petunia flowers. Plant Cell **4**: 983–993.

Bai, Y., Falk, S., Schnittger, A., Jakoby, M.J., and Hülskamp, M. (2010). Tissue layer specific regulation of leaf length and width in Arabidopsis as revealed by the cell autonomous action of ANGUSTIFOLIA. Plant J **61**: 191–199.

Berardi, A.E., Esfeld, K., Jäggi, L., Mandel, T., Cannarozzi, G.M., and Kuhlemeier, C. (2021). Complex evolution of novel red floral color in Petunia. Plant Cell **33**: 2273–2295.

Bissell, E.K. and Diggle, P.K. (2008). Floral Morphology in Nicotiana: Architectural and Temporal Effects on Phenotypic Integration. International Journal of Plant Sciences **169**: 225–240.

Bombarely, A. et al. (2016). Insight into the evolution of the Solanaceae from the parental genomes of Petunia hybrida. Nat Plants **2**: 16074.

Bouhidel, K. and Irish, V.F. (1996). Cellular Interactions Mediated by the HomeoticPISTILLATAGene Determine Cell Fate in theArabidopsisFlower. Developmental Biology **174**: 22–31.

Brandoli, C., Petri, C., Egea-Cortines, M., and Weiss, J. (2020). The clock gene Gigantea 1 from Petunia hybrida coordinates vegetative growth and inflorescence architecture. Sci Rep **10**: 275.

Cañas, L.A., Busscher, M., Angenent, G.C., Beltrán, J.-P., and Tunen, A.J.V. (1994). Nuclear localization of the petunia MADS box protein FBP1. The Plant Journal **6**: 597–604.

Cartolano, M., Castillo, R., Efremova, N., Kuckenberg, M., Zethof, J., Gerats, T., Schwarz-Sommer, Z., and Vandenbussche, M. (2007). A conserved microRNA module exerts homeotic control over Petunia hybrida and Antirrhinum majus floral organ identity. Nat Genet **39**: 901–905.

Cavallini-Speisser, Q., Morel, P., and Monniaux, M. (2021). Petal Cellular Identities. Front Plant Sci **12**: 745507.

Coen, E.S. and Meyerowitz, E.M. (1991). The war of the whorls: genetic interactions controlling flower development. Nature **353**: 31–37.

De Keukeleire, P., Maes, T., Sauer, M., Zethof, J., Van Montagu, M., and Gerats, T. (2001). Analysis by Transposon Display of the behavior of the dTph1 element family during ontogeny and inbreeding of Petunia hybrida. Mol Genet Genomics **265**: 72–81.

Dudchenko, O. et al. (2018). The Juicebox Assembly Tools module facilitates de novo assembly of mammalian genomes with chromosome-length scaffolds for under $1000. bioRxiv: 254797.

Dudchenko, O., Batra, S.S., Omer, A.D., Nyquist, S.K., Hoeger, M., Durand, N.C., Shamim, M.S., Machol, I., Lander, E.S., Aiden, A.P., and Aiden, E.L. (2017). De novo assembly of the Aedes aegypti genome using Hi-C yields chromosome-length scaffolds. Science **356**: 92–95.

Edwards, K., Johnstone, C., and Thompson, C. (1991). A simple and rapid method for the preparation of plant genomic DNA for PCR analysis. Nucleic Acids Res **19**: 1349.

Efremova, N., Perbal, M.-C., Yephremov, A., Hofmann, W.A., Saedler, H., and Schwarz-Sommer, Z. (2001). Epidermal control of floral organ identity by class B homeotic genes in Antirrhinum and Arabidopsis. Development **128**: 2661–2671.
Esfeld, K., Berardi, A.E., Moser, M., Bossolini, E., Freitas, L., and Kuhlemeier, C. (2018). Pseudogenization and Resurrection of a Speciation Gene. Curr. Biol. **28**: 3776-3786.e7.
Fornes, O. et al. (2020). JASPAR 2020: update of the open-access database of transcription factor binding profiles. Nucleic Acids Res **48**: D87–D92.
Frank, M.H. and Chitwood, D.H. (2016). Plant chimeras: The good, the bad, and the "Bizzaria." Dev. Biol. **419**: 41–53.
Galliot, C., Stuurman, J., and Kuhlemeier, C. (2006). The genetic dissection of floral pollination syndromes. Curr Opin Plant Biol **9**: 78–82.
Gerats, A.G., Huits, H., Vrijlandt, E., Marana, C., Souer, E., and Beld, M. (1990). Molecular characterization of a nonautonomous transposable element (dTph1) of petunia. Plant Cell **2**: 1121–1128.
Graeff, M., Rana, S., Marhava, P., Moret, B., and Hardtke, C.S. (2020). Local and Systemic Effects of Brassinosteroid Perception in Developing Phloem. Curr Biol **30**: 1626-1638.e3.
Hamant, O., Heisler, M.G., Jönsson, H., Krupinski, P., Uyttewaal, M., Bokov, P., Corson, F., Sahlin, P., Boudaoud, A., Meyerowitz, E.M., Couder, Y., and Traas, J. (2008). Developmental patterning by mechanical signals in Arabidopsis. Science **322**: 1650–1655.
Heberle, H., Meirelles, G.V., da Silva, F.R., Telles, G.P., and Minghim, R. (2015). InteractiVenn: a web-based tool for the analysis of sets through Venn diagrams. BMC Bioinformatics **16**: 169.
Heijmans, K., Ament, K., Rijpkema, A.S., Zethof, J., Wolters-Arts, M., Gerats, T., and Vandenbussche, M. (2012a). Redefining C and D in the petunia ABC. Plant Cell **24**: 2305–2317.
Heijmans, K., Ament, K., Rijpkema, A.S., Zethof, J., Wolters-Arts, M., Gerats, T., and Vandenbussche, M. (2012b). Redefining C and D in the petunia ABC. Plant Cell **24**: 2305–2317.
Hill, T.A., Day, C.D., Zondlo, S.C., Thackeray, A.G., and Irish, V.F. (1998). Discrete spatial and temporal cis-acting elements regulate transcription of the Arabidopsis floral homeotic gene APETALA3. Development **125**: 1711–1721.
Hoballah, M.E., Gubitz, T., Stuurman, J., Broger, L., Barone, M., Mandel, T., Dell'Olivo, A., Arnold, M., and Kuhlemeier, C. (2007). Single gene-mediated shift in pollinator attraction in Petunia. Plant Cell **19**: 779–790.
van Houwelingen, A., Souer, E., Mol, J., and Koes, R. (1999). Epigenetic interactions among three dTph1 transposons in two homologous chromosomes activate a new excision-repair mechanism in petunia. Plant Cell **11**: 1319–1336.
Hsu, H.-F., Chen, W.-H., Shen, Y.-H., Hsu, W.-H., Mao, W.-T., and Yang, C.-H. (2021). Multifunctional evolution of B and AGL6 MADS box genes in orchids. Nat Commun **12**: 902.
Jenik, P.D. and Irish, V.F. (2000). Regulation of cell proliferation patterns by homeotic genes during Arabidopsis floral development. Development **127**: 1267–1276.
Jenik, P.D. and Irish, V.F. (2001). The Arabidopsis floral homeotic gene APETALA3 differentially regulates intercellular signaling required for petal and stamen development. Development **128**: 13–23.
Kent, W.J. (2002). BLAT—The BLAST-Like Alignment Tool. Genome Res. **12**: 656–664.
Kierzkowski, D., Lenhard, M., Smith, R., and Kuhlemeier, C. (2013). Interaction between meristem tissue layers controls phyllotaxis. Dev Cell **26**: 616–628.
Kim, D., Langmead, B., and Salzberg, S.L. (2015). HISAT: a fast spliced aligner with low memory requirements. Nat Methods **12**: 357–360.

Kostyun, J.L., Gibson, M.J.S., King, C.M., and Moyle, L.C. (2019). A simple genetic architecture and low constraint allow rapid floral evolution in a diverse and recently radiating plant genus. New Phytol **223**: 1009–1022.
Krieger, G., Lupo, O., Wittkopp, P., and Barkai, N. (2022). Evolution of transcription factor binding through sequence variations and turnover of binding sites. Genome Res **32**: 1099–1111.
van der Krol, A.R., Brunelle, A., Tsuchimoto, S., and Chua, N.H. (1993). Functional analysis of petunia floral homeotic MADS box gene pMADS1. Genes Dev **7**: 1214–1228.
Kutschera, U. and Niklas, K.J. (2007). The epidermal-growth-control theory of stem elongation: an old and a new perspective. J. Plant Physiol. **164**: 1395–1409.
Lassmann, T. (2019). Kalign 3: multiple sequence alignment of large data sets. Bioinformatics **36**: 1928–1929.
Liao, Y., Smyth, G.K., and Shi, W. (2014). featureCounts: an efficient general purpose program for assigning sequence reads to genomic features. Bioinformatics **30**: 923–930.
Love, M.I., Huber, W., and Anders, S. (2014). Moderated estimation of fold change and dispersion for RNA-seq data with DESeq2. Genome Biol **15**: 550.
Lu, P., Porat, R., Nadeau, J.A., and O'Neill, S.D. (1996). Identification of a meristem L1 layer-specific gene in Arabidopsis that is expressed during embryonic pattern formation and defines a new class of homeobox genes. Plant Cell **8**: 2155–2168.
Madeira, F., Pearce, M., Tivey, A.R.N., Basutkar, P., Lee, J., Edbali, O., Madhusoodanan, N., Kolesnikov, A., and Lopez, R. (2022). Search and sequence analysis tools services from EMBL-EBI in 2022. Nucleic Acids Res **50**: W276–W279.
Martin, M. (2011). Cutadapt removes adapter sequences from high-throughput sequencing reads. EMBnet.journal **17**: 10–12.
Mayor, C., Brudno, M., Schwartz, J.R., Poliakov, A., Rubin, E.M., Frazer, K.A., Pachter, L.S., and Dubchak, I. (2000). VISTA : visualizing global DNA sequence alignments of arbitrary length. Bioinformatics **16**: 1046–1047.
McHale, N.A. and Marcotrigiano, M. (1998). LAM1 is required for dorsoventrality and lateral growth of the leaf blade in Nicotiana. Development **125**: 4235–4243.
Melzer, R., Verelst, W., and Theissen, G. (2009). The class E floral homeotic protein SEPALLATA3 is sufficient to loop DNA in 'floral quartet'-like complexes in vitro. Nucleic Acids Res. **37**: 144–157.
Meyerowitz, E.M. (1997). Genetic control of cell division patterns in developing plants. Cell **88**: 299–308.
Morel, P., Chambrier, P., Boltz, V., Chamot, S., Rozier, F., Rodrigues Bento, S., Trehin, C., Monniaux, M., Zethof, J., and Vandenbussche, M. (2019). Divergent Functional Diversification Patterns in the SEP/AGL6/AP1 MADS-Box Transcription Factor Superclade. Plant Cell **31**: 3033–3056.
Morel, P., Heijmans, K., Rozier, F., Zethof, J., Chamot, S., Bento, S.R., Vialette-Guiraud, A., Chambrier, P., Trehin, C., and Vandenbussche, M. (2017). Divergence of the Floral A-Function between an Asterid and a Rosid Species. Plant Cell **29**: 1605–1621.
Moyroud, E. and Glover, B.J. (2017). The Evolution of Diverse Floral Morphologies. Curr. Biol. **27**: R941–R951.
Perbal, M.C., Haughn, G., Saedler, H., and Schwarz-Sommer, Z. (1996). Non-cell-autonomous function of the Antirrhinum floral homeotic proteins DEFICIENS and GLOBOSA is exerted by their polar cell-to-cell trafficking. Development **122**: 3433–3441.
Purugganan, M.D., Rounsley, S.D., Schmidt, R.J., and Yanofsky, M.F. (1995). Molecular evolution of flower development: diversification of the plant MADS-box regulatory gene family. Genetics **140**: 345–356.

Quattrocchio, F., Wing, J., van der Woude, K., Souer, E., de Vetten, N., Mol, J., and Koes, R. (1999). Molecular analysis of the anthocyanin2 gene of petunia and its role in the evolution of flower color. Plant Cell **11**: 1433–1444.
Quattrocchio, F., Wing, J.F., Leppen, H.T.C., Mol, J.N.M., and Koes, R.E. (1993). Regulatory Genes Controlling Anthocyanin Pigmentation Are Functionally Conserved among Plant Species and Have Distinct Sets of Target Genes. Plant Cell **5**: 1497–1512.
Quattrocchio, F., Wing, J.F., van der Woude, K., Mol, J.N., and Koes, R. (1998). Analysis of bHLH and MYB domain proteins: species-specific regulatory differences are caused by divergent evolution of target anthocyanin genes. Plant J **13**: 475–488.
Reale, L., Porceddu, A., Lanfaloni, L., Moretti, C., Zenoni, S., Pezzotti, M., Romano, B., and Ferranti, F. (2002). Patterns of cell division and expansion in developing petals of Petunia hybrida. Sex Plant Reprod **15**: 123–132.
Reck-Kortmann, M., Silva-Arias, G.A., Segatto, A.L.A., Mader, G., Bonatto, S.L., and de Freitas, L.B. (2014). Multilocus phylogeny reconstruction: new insights into the evolutionary history of the genus Petunia. Mol Phylogenet Evol **81**: 19–28.
Ren, H., Dang, X., Cai, X., Yu, P., Li, Y., Zhang, S., Liu, M., Chen, B., and Lin, D. (2017). Spatio-temporal orientation of microtubules controls conical cell shape in Arabidopsis thaliana petals. PLOS Genetics **13**: e1006851.
Riechmann, J.L., Krizek, B.A., and Meyerowitz, E.M. (1996a). Dimerization specificity of Arabidopsis MADS domain homeotic proteins APETALA1, APETALA3, PISTILLATA, and AGAMOUS. Proc Natl Acad Sci U S A **93**: 4793–4798.
Riechmann, J.L., Wang, M., and Meyerowitz, E.M. (1996b). DNA-binding properties of Arabidopsis MADS domain homeotic proteins APETALA1, APETALA3, PISTILLATA and AGAMOUS. Nucleic Acids Res **24**: 3134–3141.
Rijpkema, A.S., Royaert, S., Zethof, J., Weerden, G. van der, Gerats, T., and Vandenbussche, M. (2006). Analysis of the Petunia TM6 MADS Box Gene Reveals Functional Divergence within the DEF/AP3 Lineage. The Plant Cell **18**: 1819–1832.
Sandelin, A., Alkema, W., Engström, P., Wasserman, W.W., and Lenhard, B. (2004). JASPAR: an open-access database for eukaryotic transcription factor binding profiles. Nucleic Acids Res **32**: D91-94.
Satina, S. and Blakeslee, A.F. (1941). Periclinal Chimeras in Datura Stramonium in Relation to Development of Leaf and Flower. American Journal of Botany **28**: 862–871.
Satina, S., Blakeslee, A.F., and Avery, A.G. (1940). Demonstration of the Three Germ Layers in the Shoot Apex of Datura by Means of Induced Polyploidy in Periclinal Chimeras. American Journal of Botany **27**: 895–905.
Savaldi-Goldstein, S., Peto, C., and Chory, J. (2007). The epidermis both drives and restricts plant shoot growth. Nature **446**: 199–202.
Scheres, B. (2001). Plant cell identity. The role of position and lineage. Plant Physiol **125**: 112–114.
Schmidt, D. et al. (2010). Five-vertebrate ChIP-seq reveals the evolutionary dynamics of transcription factor binding. Science **328**: 1036–1040.
Schwarz-Sommer, Z., Hue, I., Huijser, P., Flor, P.J., Hansen, R., Tetens, F., Lönnig, W.E., Saedler, H., and Sommer, H. (1992). Characterization of the Antirrhinum floral homeotic MADS-box gene deficiens: evidence for DNA binding and autoregulation of its persistent expression throughout flower development. EMBO J. **11**: 251–263.
Schwarz-Sommer, Z., Huijser, P., Nacken, W., Saedler, H., and Sommer, H. (1990). Genetic Control of Flower Development by Homeotic Genes in Antirrhinum majus. Science **250**: 931–936.

Sierro, N., Battey, J.N.D., Ouadi, S., Bakaher, N., Bovet, L., Willig, A., Goepfert, S., Peitsch, M.C., and Ivanov, N.V. (2014). The tobacco genome sequence and its comparison with those of tomato and potato. Nat Commun **5**: 3833.
Silva, C.S., Puranik, S., Round, A., Brennich, M., Jourdain, A., Parcy, F., Hugouvieux, V., and Zubieta, C. (2015). Evolution of the Plant Reproduction Master Regulators LFY and the MADS Transcription Factors: The Role of Protein Structure in the Evolutionary Development of the Flower. Front Plant Sci **6**: 1193.
Slater, G.S.C. and Birney, E. (2005). Automated generation of heuristics for biological sequence comparison. BMC Bioinformatics **6**: 31.
Solomon, E.R., Caldwell, K.K., and Allan, A.M. (2021). A novel method for the normalization of ChIP-qPCR data. MethodsX **8**: 101504.
Spelt, C., Quattrocchio, F., Mol, J.N.M., and Koes, R. (2000). anthocyanin1 of Petunia Encodes a Basic Helix-Loop-Helix Protein That Directly Activates Transcription of Structural Anthocyanin Genes. The Plant Cell **12**: 1619–1631.
Stewart, R.N. and Burk, L.G. (1970). Independence of Tissues Derived from Apical Layers in Ontogeny of the Tobacco Leaf and Ovary. American Journal of Botany **57**: 1010–1016.
Stormo, G.D. (2013). Modeling the specificity of protein-DNA interactions. Quant Biol **1**: 115–130.
Stuurman, J., Hoballah, M.E., Broger, L., Moore, J., Basten, C., and Kuhlemeier, C. (2004). Dissection of floral pollination syndromes in Petunia. Genetics **168**: 1585–1599.
Takatani, S., Verger, S., Okamoto, T., Takahashi, T., Hamant, O., and Motose, H. (2020). Microtubule Response to Tensile Stress Is Curbed by NEK6 to Buffer Growth Variation in the Arabidopsis Hypocotyl. Curr Biol **30**: 1491-1503.e2.
Terry, M.I., Pérez-Sanz, F., Díaz-Galián, M.V., Pérez de Los Cobos, F., Navarro, P.J., Egea-Cortines, M., and Weiss, J. (2019). The Petunia CHANEL Gene is a ZEITLUPE Ortholog Coordinating Growth and Scent Profiles. Cells **8**.
Theißen, G., Kim, J.T., and Saedler, H. (1996). Classification and phylogeny of the MADS-box multigene family suggest defined roles of MADS-box gene subfamilies in the morphological evolution of eukaryotes. J Mol Evol **43**: 484–516.
Tilney-Bassett, R.A.E. (1986). Plant chimeras (E. Arnold: London ; Baltimore, Md., U.S.A).
Tornielli, G., Koes, R., and Quattrocchio, F. (2009). The Genetics of Flower Color. In Petunia: Evolutionary, Developmental and Physiological Genetics, T. Gerats and J. Strommer, eds (Springer: New York, NY), pp. 269–299.
Tröbner, W., Ramirez, L., Motte, P., Hue, I., Huijser, P., Lönnig, W.E., Saedler, H., Sommer, H., and Schwarz-Sommer, Z. (1992). GLOBOSA: a homeotic gene which interacts with DEFICIENS in the control of Antirrhinum floral organogenesis. EMBO J **11**: 4693–4704.
Urbanus, S.L., Dinh, Q.D.P., Angenent, G.C., and Immink, R.G.H. (2010a). Investigation of MADS domain transcription factor dynamics in the floral meristem. Plant Signal Behav **5**: 1260–1262.
Urbanus, S.L., Martinelli, A.P., Dinh, Q.D.P., Aizza, L.C.B., Dornelas, M.C., Angenent, G.C., and Immink, R.G.H. (2010b). Intercellular transport of epidermis-expressed MADS domain transcription factors and their effect on plant morphology and floral transition. Plant J **63**: 60–72.
Vandenbussche, M., Horstman, A., Zethof, J., Koes, R., Rijpkema, A.S., and Gerats, T. (2009). Differential recruitment of WOX transcription factors for lateral development and organ fusion in Petunia and Arabidopsis. Plant Cell **21**: 2269–2283.
Vandenbussche, M., Janssen, A., Zethof, J., van Orsouw, N., Peters, J., van Eijk, M.J.T., Rijpkema, A.S., Schneiders, H., Santhanam, P., de Been, M., van Tunen, A., and Gerats, T. (2008). Generation of a 3D indexed Petunia insertion database for reverse genetics. Plant J **54**: 1105–1114.

Vandenbussche, M., Zethof, J., Royaert, S., Weterings, K., and Gerats, T. (2004). The duplicated B-class heterodimer model: whorl-specific effects and complex genetic interactions in Petunia hybrida flower development. Plant Cell **16**: 741–754.
Venail, J., Dell'olivo, A., and Kuhlemeier, C. (2010). Speciation genes in the genus Petunia. Philos Trans R Soc Lond B Biol Sci **365**: 461–468.
de Vetten, N., Quattrocchio, F., Mol, J., and Koes, R. (1997). The an11 locus controlling flower pigmentation in petunia encodes a novel WD-repeat protein conserved in yeast, plants, and animals. Genes Dev **11**: 1422–1434.
Vincent, C.A., Carpenter, R., and Coen, E.S. (2003). Interactions between gene activity and cell layers during floral development. The Plant Journal **33**: 765–774.
de Vlaming, P., Gerats, A.G.M., Wiering, H., Wijsman, H.J.W., Cornu, A., Farcy, E., and Maizonnier, D. (1984). Petunia hybrida: A short description of the action of 91 genes, their origin and their map location. Plant Mol Biol Rep **2**: 21–42.
Wuest, S.E., O'Maoileidigh, D.S., Rae, L., Kwasniewska, K., Raganelli, A., Hanczaryk, K., Lohan, A.J., Loftus, B., Graciet, E., and Wellmer, F. (2012). Molecular basis for the specification of floral organs by APETALA3 and PISTILLATA. Proc. Natl. Acad. Sci. U.S.A. **109**: 13452–13457.
Yadav, R.K., Tavakkoli, M., Xie, M., Girke, T., and Reddy, G.V. (2014). A high-resolution gene expression map of the Arabidopsis shoot meristem stem cell niche. Development **141**: 2735–2744.
Zenoni, S., Reale, L., Tornielli, G.B., Lanfaloni, L., Porceddu, A., Ferrarini, A., Moretti, C., Zamboni, A., Speghini, A., Ferranti, F., and Pezzotti, M. (2004). Downregulation of the Petunia hybrida alpha-expansin gene PhEXP1 reduces the amount of crystalline cellulose in cell walls and leads to phenotypic changes in petal limbs. Plant Cell **16**: 295–308.
Zhang, B., Xu, X., Huang, R., Yang, S., Li, M., and Guo, Y. (2021). CRISPR/Cas9-mediated targeted mutation reveals a role for AN4 rather than DPL in regulating venation formation in the corolla tube of Petunia hybrida. Hortic Res **8**: 116.
Zhao, F. et al. (2020). Microtubule-Mediated Wall Anisotropy Contributes to Leaf Blade Flattening. Curr Biol **30**: 3972-3985.e6.

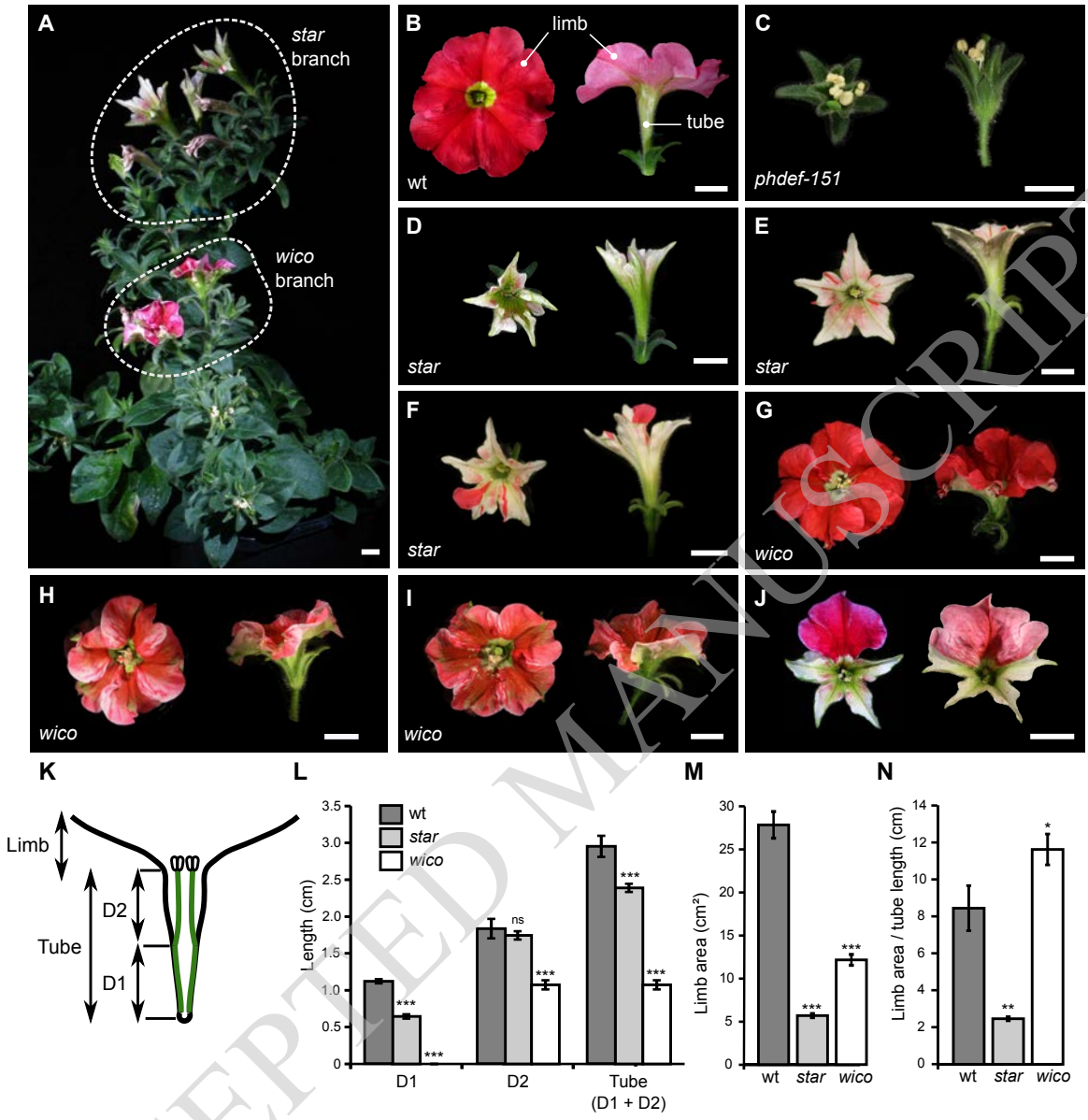

Figure 1. Macroscopic description of the *star* and *wico* flowers.
(A) *phdef-151* mutant plant harboring one branch with *wico* revertant flowers and one branch with *star* revertant flowers. Scale bar: 1 cm. **(B-I)** Representative wild-type (wt) (B), *phdef-151* (C), *star* (D-F) and *wico* (G-I) flowers from a top (left) and side (right) view. The *star* and *wico* flowers come from independent reversion events (from different *phdef-151* plants or from different branches of a single *phdef-151* plant). Scale bar: 1 cm. **(J)** Two *star* flowers with additional L1-revertant sectors in one petal (left) or one petal and two half petals (right). Scale bar: 1 cm. **(K)** Schematic cross-section of a wt flower, showing stamens (in green) partially fused to the petal tube. The region of the tube fused to stamens is named D1, and the region of the tube where stamens are free is named D2, as defined in (Stuurman et al., 2004). **(L)** Average length of regions D1, D2 and total tube length in wt, *star* and *wico* flowers. **(M)** Average limb area in wt, *star* and *wico* flowers. **(N)** Average ratio between limb area and tube length in wt, *star* and *wico* flowers. n = 7 wt flowers, n = 12 *star* flowers from 4 different branches, n = 18 *wico* flowers from 5 different branches. Student's t test, two-sided with Welch correction for D1, D2 and tube length, two-sided without Welch correction for limb area and limb area/tube length ratio (* $p < 0.05$, ** $p < 0.01$, *** $p < 0.005$). Error bars represent ± s.e.m.

A

B

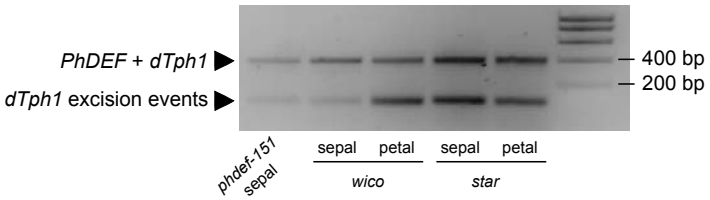

C

Phenotype	Allele	Nucleotidic sequence	Protein Sequence	n
wt	*PhDEF*	CCAGTA------CTGG--------CAAGCTTCAT	DAKVSIIMISS--TG--KLHEFIS	
phdef	*phdef(+8)*	CCAGTA------CTGGCAGTCTGGCAAGCTTCAT	DAKVSIIMISS--TGSLASFMNSL(+22aa)*	1
	phdef(+7)	CCAGTA------CTGGC-GTCTGGCAAGCTTCAT	DAKVSIIMISS--TGVWQAS*	1
star	*PhDEF*	CCAGTA------CTGG--------CAAGCTTCAT	DAKVSIIMISS--TG--KLHEFIS	1
	phdef (+6a)	CCAGTA------CTGG--GTCTGGCAAGCTTCAT	DAKVSIIMISS--TGSGKLHEFIS	7
	phdef (+6b)	CCAGTA------CTGGCA-T-TGGCAAGCTTCAT	DAKVSIIMISS--TGIGKLHEFIS	6
wico	*PhDEF*	CCAGTA------CTGG--------CAAGCTTCAT	DAKVSIIMISS--TG--KLHEFIS	3
	phdef (+6a)	CCAGTA------CTGG--GTCTGGCAAGCTTCAT	DAKVSIIMISS--TGSGKLHEFIS	7
	phdef (+6c)	CCAGTA------CTGGCA--CTGGCAAGCTTCAT	DAKVSIIMISS--TGTGKLHEFIS	3
	phdef (+6d)	CCAGTAGCCAGTCTGG--------CAAGCTTCAT	DAKVSIIMISSSQSG--KLHEFIS	1

Figure 2. Sequencing the *PhDEF* excision alleles in *star* and *wico* flowers.
(A) *PhDEF* gene model indicating the position of the *dTph1* insertion in the first exon (black triangle) and the primers used for subsequent amplification and sequencing (in red). **(B)** Amplicons generated with primers spanning the *dTph1* insertion site, on genomic DNA from *phdef-151* second whorl organs and *star* and *wico* sepals and petals. The large fragment still contains the *dTph1* transposon inserted (expected size: 407 bp), while small fragments result from different events of *dTph1* excision (expected size: 115 bp) and were subsequently sequenced. **(C)** The small *PhDEF* fragments from (B) were sequenced in the second whorl organs of flowers with a *phdef* (n = 2), *star* (n = 14) and *wico* (n = 14) phenotype. The nucleotidic sequence and predicted protein sequence are indicated, with stop codons represented by a *star*. Additional nucleotides or amino-acids as compared to the wt sequences are indicated in red. n = number of independent reversion events where the same excision footprint was found. wt = wild-type.

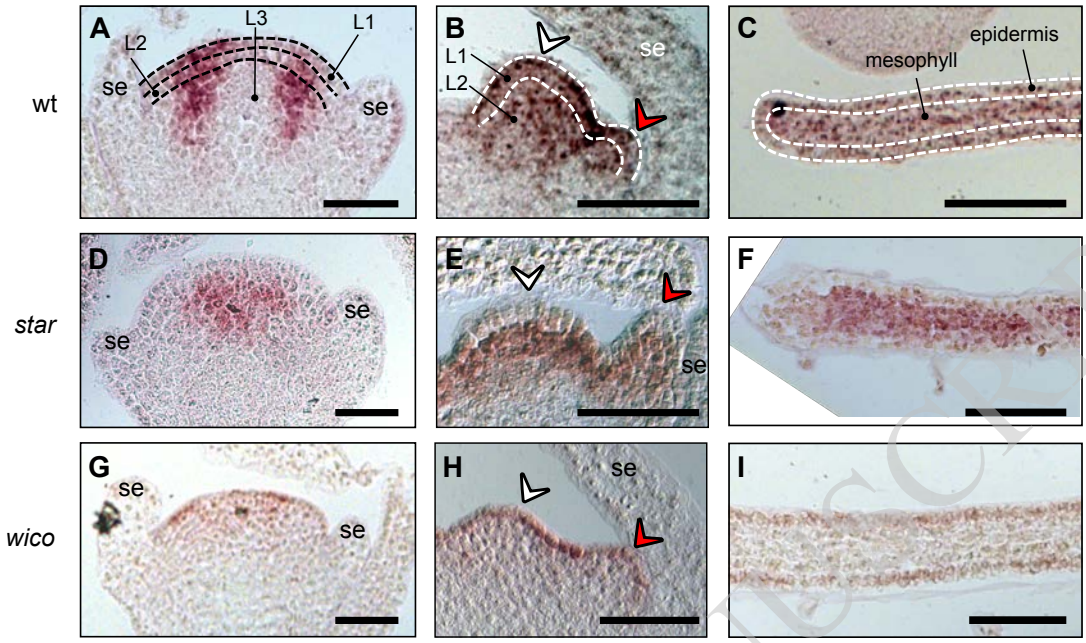

Figure 3. Localization of the *PhDEF* transcript in wt, *star* and *wico* flowers by *in situ* hybridization.

Longitudinal sections of wild-type (wt) (A, B, C), *star* (D, E, F) and *wico* (G, H, I) flowers or young petals hybridized with a digoxigenin-labelled *PhDEF* antisense probe. At the earliest stage chosen (A, D, G), sepals are initiating and *PhDEF* is expressed in the future petal / stamen initiation domain. Note that if the section was not performed at the center of the flower, the *PhDEF* signal might artificially appear to be in the middle of the flower (as in D) whereas it is actually on its flanks. At the middle stage chosen (B, E, H), stamens (white arrowhead) and petals (red arrowhead) are initiating, and *PhDEF* is expressed in both primordia. The meristematic L1, L2 and L3 layers are indicated on the wt sections (A, B). *PhDEF* expression is also detected at the tip of young petal limb (C, F, I). The epidermis and mesophyll layers, derived from the previous L1 and L2 meristematic layers, are indicated on the wt section (C). se: sepals. Scale bar: 50 µm.

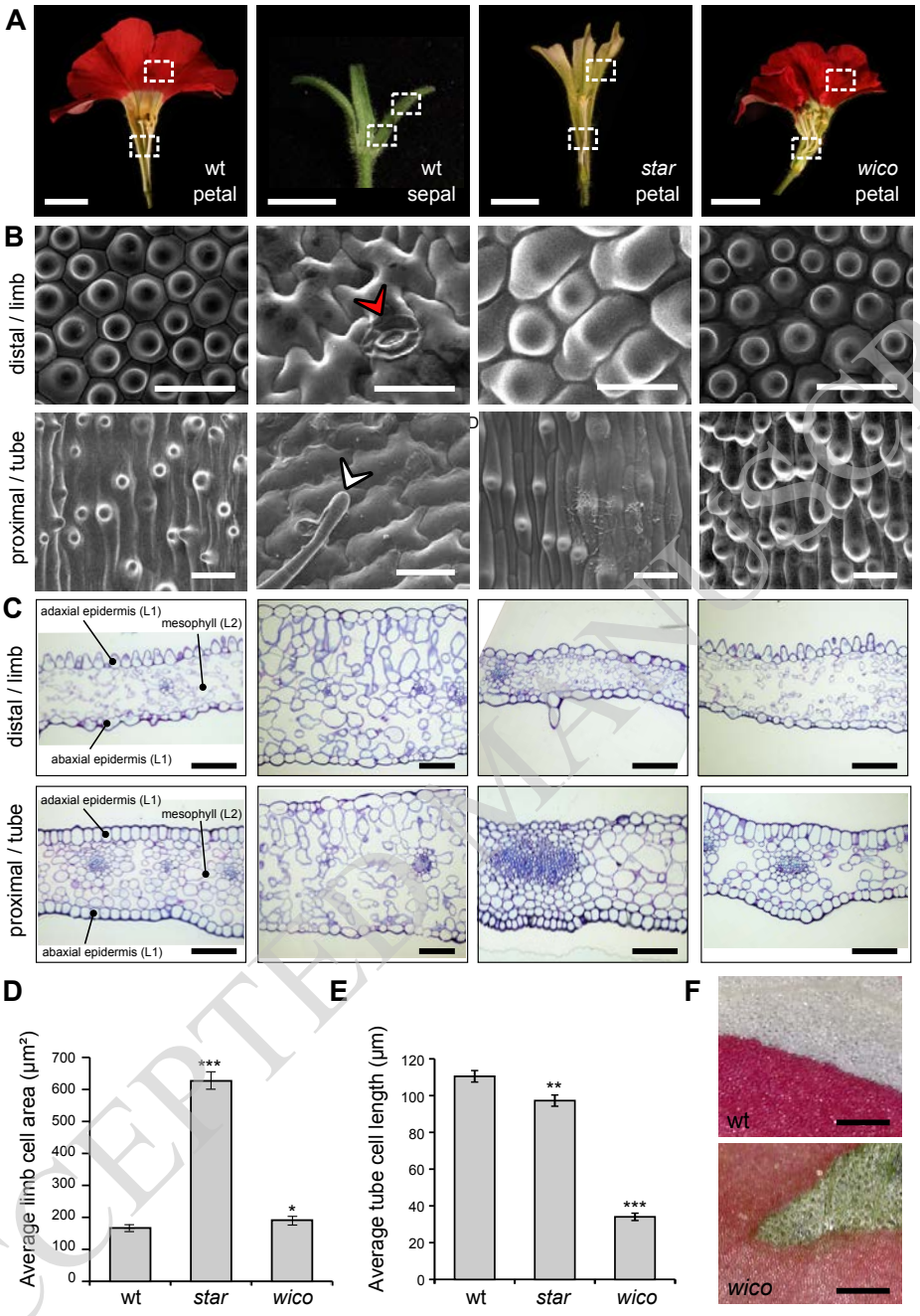

Figure 4. Epidermal and mesophyll cell identities in wt petals and sepals, and *star* and *wico* petals.

(A) From left to right: wild-type (wt) petals, wt sepals, *star* petals and *wico* petals cut open longitudinally to show areas used for scanning electron microscopy and cross-sections. Petals were subdivided into limb and tube area, and sepals were subdivided into a distal and a proximal part, as shown by the dotted white rectangles. Scale bar: 1 cm. **(B)** Representative scanning electron micrographs from the adaxial side of a wt petal, wt sepal, *star* petal and *wico* petal (from left to right). The red arrowhead points to a stomata and the white arrowhead points to a trichome. Scale bar: 30 µm. **(C)** Representative cross-sections from wt petals, wt sepals, *star* petals and *wico* petals (from left to right) stained with toluidine blue. The adaxial and abaxial epidermis and the mesophyll are indicated on the wt petal sections. Scale bar: 100 µm. **(D)** Average limb cell area from the adaxial side of wt, *star* and *wico* petals (n = 30 cells). Student's t test with Welch correction, two-sided (* $p < 0.05$, ** $p < 0.01$, *** $p < 0.005$). Error bars represent ± s.e.m. **(E)** Average tube cell length from the adaxial side of wt, *star* and *wico* petals (n = 40 cells for wt, 45 cells for *star* and *wico*). Wilcoxon rank sum test, two-sided (* $p < 0.05$, ** $p < 0.01$, *** $p < 0.005$). Error bars represent ± s.e.m. **(F)** Limb area from wt (top) and *wico* (bottom) petals, after their adaxial epidermis was manually peeled. For wt, the upper half of the picture shows the white underlying mesophyll. For *wico*, the green triangular area shows the green (chloroplastic) underlying mesophyll. Scale bar: 300 µm.

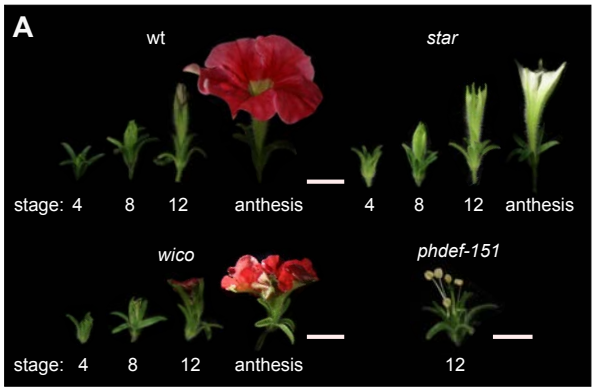

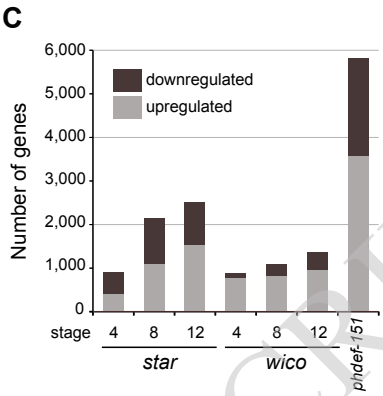

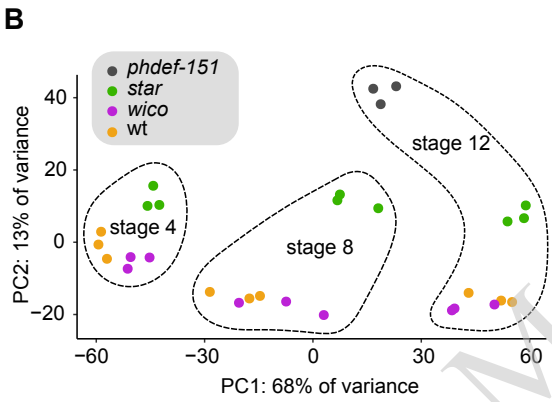

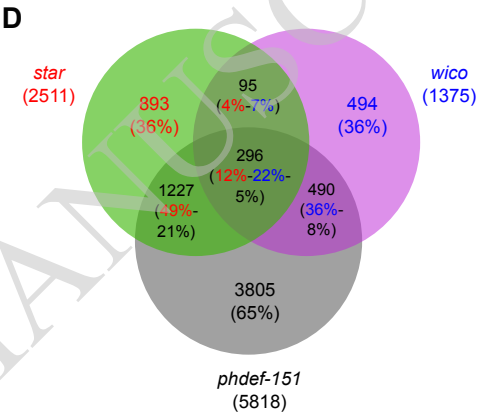

Figure 5. Gene differential expression in *star* and *wico* petals.
(A) Flowers from wild-type (wt), *star*, *wico* and *phdef-151* at stages 4, 8 and 12 (only stage 12 for *phdef-151*), whose petals or sepals were harvested for transcriptome sequencing. Flowers at anthesis are shown for comparison. Scale bar: 1 cm. **(B)** Principal Component Analysis plot of the samples after analysis of variance with DESeq2, showing that the first principal component corresponds to the developmental stage and the second principal component corresponds to the genotype. **(C)** Number of upregulated and downregulated genes in *star*, *wico* and *phdef-151*, as compared to wt at the corresponding stages. **(D)** Venn diagram recapitulating the number of differentially expressed genes (DEGs) in *star*, *wico* and *phdef-151* petal samples at stage 12, as compared to wt, and their different intersections. Each sector contains the number of DEGs, and between parenthesis is the percentage of genes that it represents from the total number of DEGs in the corresponding sample, with a colour code (red = percentage of DEGs from *star* samples / blue = from *wico* samples / black = from *phdef-151* samples).

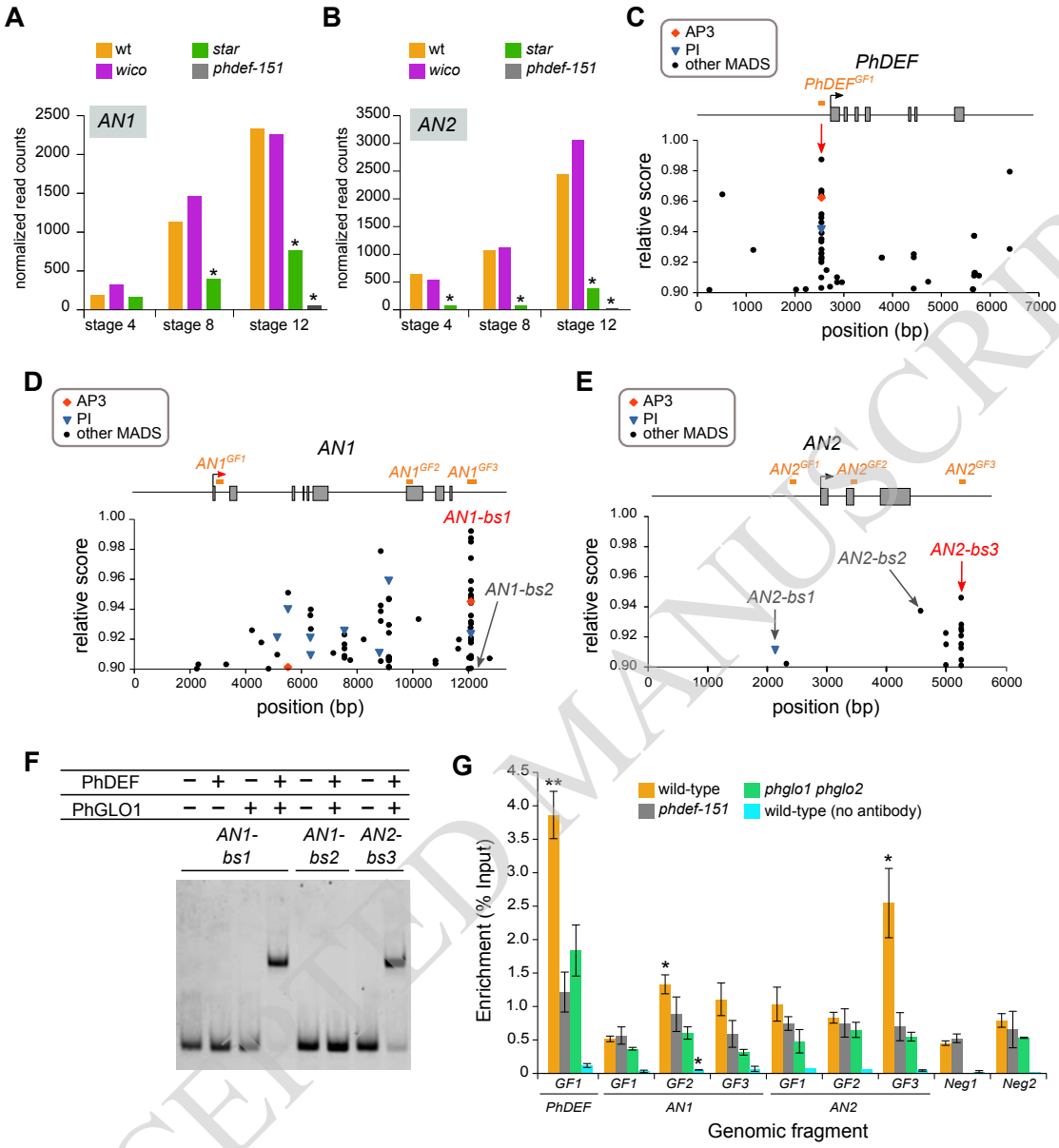

Figure 6. PhDEF binds to *AN2* regulatory region *in vitro* and *in vivo*.
(A, B) Expression (as normalized read counts calculated by DESeq2) of *AN1* (A) and *AN2* (B) in wild-type (wt), *star*, *wico* and *phdef-151* second whorl organs at stages 4, 8 or 12. Stars indicate significant down-regulation (log2FC < -1 and adjusted p-value < 0.01). **(C-E)** Relative score profiles for AP3 (red diamond), PI (blue triangle) and all other MADS-box transcription factors (black dots) available on Jaspar, on the genomic sequences of *PhDEF* (C), *AN1* (D) and *AN2* (E). The relative score is computed using the position weight matrix of each transcription factor and is between 0 and 1; only relative scores higher than 0.86 are shown here. The gene model is represented above the score profile with exons as grey rectangles, the transcription start site as an arrow, and the gene model is aligned with the position of the predicted binding sites (bs). For *PhDEF*, the position of a putative CArG box, as explained in the main text, is indicated by a red arrow. The positions of the sites tested by gel shift in panel F and Supplemental Figure S8 are indicated: putative PhDEF binding sites (*AN1-bs1, AN2-bs1, AN2-bs2* and *AN2-bs3*) and a negative control with a low predicted binding score (*AN1-bs2)*. Sites indicated in red were bound in the gel shift assay, while sites indicated in grey were not bound. In orange, are depicted the genomic fragments (GF) tested by chromatin immunoprecipitation in (G). **(F)** Representative electrophoretic mobility shift assay (EMSA) gel performed with a combination of *in vitro*-translated PhDEF and/or PhGLO1 proteins, and Cy5-labelled *AN1-bs1, AN1-bs2* or *AN2-bs3* DNA fragments, whose position is depicted in (C-E). Similar results were obtained in 5 additional independent assays for *AN1-bs1*, 2 additional independent assays for *AN2-bs3* and 4 additional independent assays for *AN1-bs2*. **(G)** Enrichment (as percentage of INPUT) of binding of PhDEF to different genomic regions of the chromatin purified from wt, *phdef-151* or *phglo1 phglo2* second whorl organs at stage 8, after immunoprecipitation with an anti-PhDEF directed antibody. The control without antibody was performed on chromatin isolated from wt petals. The position of the genomic fragments tested is depicted in (C-E). Neg1 and Neg2 represent two negative control fragments located in the promoter region of genes not differentially expressed in the *phdef-151* mutant, and present on different chromosomes than *PhDEF*, *AN1* and *AN2.* For unknown reasons, the Neg1 control region could never be amplified in the *phglo1 phglo2* samples. *Star*s indicate a significant enrichment of test regions over the average of the two negative control regions for each chromatin sample (one-sided t-test with Welch correction, * $p<0.05$, ** $p<0.005$; n = 3 biological replicates for wt and *phdef-151*, 2 biological replicates for *phglo1 phglo2* and the control without antibody). Error bars represent ± s.e.m.

Parsed Citations

Abe, M., Takahashi, T., and Komeda, Y. (1999). Cloning and characterization of an L1 layer-specific gene in Arabidopsis thaliana. Plant Cell Physiol 40: 571–580.
Google Scholar: Author Only Title Only Author and Title

Aerts, N., de Bruijn, S., van Mourik, H., Angenent, G.C., and van Dijk, A.D.J. (2018). Comparative analysis of binding patterns of MADS-domain proteins in Arabidopsis thaliana. BMC Plant Biol 18: 1–16.
Google Scholar: Author Only Title Only Author and Title

Albert, N.W., Lewis, D.H., Zhang, H., Schwinn, K.E., Jameson, P.E., and Davies, K.M. (2011). Members of an R2R3-MYB transcription factor family in Petunia are developmentally and environmentally regulated to control complex floral and vegetative pigmentation patterning. Plant J 65: 771–784.
Google Scholar: Author Only Title Only Author and Title

Angenent, G.C., Busscher, M., Franken, J., Mol, J.N., and van Tunen, A.J. (1992). Differential expression of two MADS box genes in wild-type and mutant petunia flowers. Plant Cell 4: 983–993.
Google Scholar: Author Only Title Only Author and Title

Bai, Y., Falk, S., Schnittger, A., Jakoby, M.J., and Hülskamp, M. (2010). Tissue layer specific regulation of leaf length and width in Arabidopsis as revealed by the cell autonomous action of ANGUSTIFOLIA. Plant J 61: 191–199.
Google Scholar: Author Only Title Only Author and Title

Berardi, A.E., Esfeld, K., Jäggi, L., Mandel, T., Cannarozzi, G.M., and Kuhlemeier, C. (2021). Complex evolution of novel red floral color in Petunia. Plant Cell 33: 2273–2295.
Google Scholar: Author Only Title Only Author and Title

Bissell, E.K. and Diggle, P.K. (2008). Floral Morphology in Nicotiana: Architectural and Temporal Effects on Phenotypic Integration. International Journal of Plant Sciences 169: 225–240.
Google Scholar: Author Only Title Only Author and Title

Bombarely, A. et al. (2016). Insight into the evolution of the Solanaceae from the parental genomes of Petunia hybrida. Nat Plants 2: 16074.
Google Scholar: Author Only Title Only Author and Title

Bouhidel, K. and Irish, V.F. (1996). Cellular Interactions Mediated by the HomeoticPISTILLATAGene Determine Cell Fate in theArabidopsisFlower. Developmental Biology 174: 22–31.
Google Scholar: Author Only Title Only Author and Title

Brandoli, C., Petri, C., Egea-Cortines, M., and Weiss, J. (2020). The clock gene Gigantea 1 from Petunia hybrida coordinates vegetative growth and inflorescence architecture. Sci Rep 10: 275.
Google Scholar: Author Only Title Only Author and Title

Cañas, L.A., Busscher, M., Angenent, G.C., Beltrán, J.-P., and Tunen, A.J.V. (1994). Nuclear localization of the petunia MADS box protein FBP1. The Plant Journal 6: 597–604.
Google Scholar: Author Only Title Only Author and Title

Cartolano, M., Castillo, R., Efremova, N., Kuckenberg, M., Zethof, J., Gerats, T., Schwarz-Sommer, Z., and Vandenbussche, M. (2007). A conserved microRNA module exerts homeotic control over Petunia hybrida and Antirrhinum majus floral organ identity. Nat Genet 39: 901–905.
Google Scholar: Author Only Title Only Author and Title

Cavallini-Speisser, Q., Morel, P., and Monniaux, M. (2021). Petal Cellular Identities. Front Plant Sci 12: 745507.
Google Scholar: Author Only Title Only Author and Title

Coen, E.S. and Meyerowitz, E.M. (1991). The war of the whorls: genetic interactions controlling flower development. Nature 353: 31–37.
Google Scholar: Author Only Title Only Author and Title

De Keukeleire, P., Maes, T., Sauer, M., Zethof, J., Van Montagu, M., and Gerats, T. (2001). Analysis by Transposon Display of the behavior of the dTph1 element family during ontogeny and inbreeding of Petunia hybrida. Mol Genet Genomics 265: 72–81.
Google Scholar: Author Only Title Only Author and Title

Dudchenko, O. et al. (2018). The Juicebox Assembly Tools module facilitates de novo assembly of mammalian genomes with chromosome-length scaffolds for under $1000. bioRxiv: 254797.
Google Scholar: Author Only Title Only Author and Title

Dudchenko, O., Batra, S.S., Omer, A.D., Nyquist, S.K., Hoeger, M., Durand, N.C., Shamim, M.S., Machol, I., Lander, E.S., Aiden, A.P., and Aiden, E.L. (2017). De novo assembly of the Aedes aegypti genome using Hi-C yields chromosome-length scaffolds. Science 356: 92–95.

Google Scholar: Author Only Title Only Author and Title

Edwards, K., Johnstone, C., and Thompson, C. (1991). A simple and rapid method for the preparation of plant genomic DNA for PCR analysis. Nucleic Acids Res 19: 1349.
Google Scholar: Author Only Title Only Author and Title

Efremova, N., Perbal, M.-C., Yephremov, A., Hofmann, W.A., Saedler, H., and Schwarz-Sommer, Z. (2001). Epidermal control of floral organ identity by class B homeotic genes in Antirrhinum and Arabidopsis. Development 128: 2661–2671.
Google Scholar: Author Only Title Only Author and Title

Esfeld, K., Berardi, A.E., Moser, M., Bossolini, E., Freitas, L., and Kuhlemeier, C. (2018). Pseudogenization and Resurrection of a Speciation Gene. Curr. Biol. 28: 3776-3786.e7.
Google Scholar: Author Only Title Only Author and Title

Fornes, O. et al. (2020). JASPAR 2020: update of the open-access database of transcription factor binding profiles. Nucleic Acids Res 48: D87–D92.
Google Scholar: Author Only Title Only Author and Title

Frank, M.H. and Chitwood, D.H. (2016). Plant chimeras: The good, the bad, and the "Bizzaria." Dev. Biol. 419: 41–53.
Google Scholar: Author Only Title Only Author and Title

Galliot, C., Stuurman, J., and Kuhlemeier, C. (2006). The genetic dissection of floral pollination syndromes. Curr Opin Plant Biol 9: 78–82.
Google Scholar: Author Only Title Only Author and Title

Gerats, A.G., Huits, H., Vrijlandt, E., Marana, C., Souer, E., and Beld, M. (1990). Molecular characterization of a nonautonomous transposable element (dTph1) of petunia. Plant Cell 2: 1121–1128.
Google Scholar: Author Only Title Only Author and Title

Graeff, M., Rana, S., Marhava, P., Moret, B., and Hardtke, C.S. (2020). Local and Systemic Effects of Brassinosteroid Perception in Developing Phloem. Curr Biol 30: 1626-1638.e3.
Google Scholar: Author Only Title Only Author and Title

Hamant, O., Heisler, M.G., Jönsson, H., Krupinski, P., Uyttewaal, M., Bokov, P., Corson, F., Sahlin, P., Boudaoud, A., Meyerowitz, E.M., Couder, Y., and Traas, J. (2008). Developmental patterning by mechanical signals in Arabidopsis. Science 322: 1650–1655.
Google Scholar: Author Only Title Only Author and Title

Heberle, H., Meirelles, G.V., da Silva, F.R., Telles, G.P., and Minghim, R. (2015). InteractiVenn: a web-based tool for the analysis of sets through Venn diagrams. BMC Bioinformatics 16: 169.
Google Scholar: Author Only Title Only Author and Title

Heijmans, K., Ament, K., Rijpkema, A.S., Zethof, J., Wolters-Arts, M., Gerats, T., and Vandenbussche, M. (2012a). Redefining C and D in the petunia ABC. Plant Cell 24: 2305–2317.
Google Scholar: Author Only Title Only Author and Title

Heijmans, K., Ament, K., Rijpkema, A.S., Zethof, J., Wolters-Arts, M., Gerats, T., and Vandenbussche, M. (2012b). Redefining C and D in the petunia ABC. Plant Cell 24: 2305–2317.
Google Scholar: Author Only Title Only Author and Title

Hill, T.A., Day, C.D., Zondlo, S.C., Thackeray, A.G., and Irish, V.F. (1998). Discrete spatial and temporal cis-acting elements regulate transcription of the Arabidopsis floral homeotic gene APETALA3. Development 125: 1711–1721.
Google Scholar: Author Only Title Only Author and Title

Hoballah, M.E., Gubitz, T., Stuurman, J., Broger, L., Barone, M., Mandel, T., Dell'Olivo, A., Arnold, M., and Kuhlemeier, C. (2007). Single gene-mediated shift in pollinator attraction in Petunia. Plant Cell 19: 779–790.
Google Scholar: Author Only Title Only Author and Title

van Houwelingen, A., Souer, E., Mol, J., and Koes, R. (1999). Epigenetic interactions among three dTph1 transposons in two homologous chromosomes activate a new excision-repair mechanism in petunia. Plant Cell 11: 1319–1336.
Google Scholar: Author Only Title Only Author and Title

Hsu, H.-F., Chen, W.-H., Shen, Y.-H., Hsu, W.-H., Mao, W.-T., and Yang, C.-H. (2021). Multifunctional evolution of B and AGL6 MADS box genes in orchids. Nat Commun 12: 902.
Google Scholar: Author Only Title Only Author and Title

Jenik, P.D. and Irish, V.F. (2000). Regulation of cell proliferation patterns by homeotic genes during Arabidopsis floral development. Development 127: 1267–1276.
Google Scholar: Author Only Title Only Author and Title

Jenik, P.D. and Irish, V.F. (2001). The Arabidopsis floral homeotic gene APETALA3 differentially regulates intercellular signaling required for petal and stamen development. Development 128: 13–23.

Google Scholar: Author Only Title Only Author and Title

Kent, W.J. (2002). BLAT-The BLAST-Like Alignment Tool. Genome Res. 12: 656–664.
Google Scholar: Author Only Title Only Author and Title

Kierzkowski, D., Lenhard, M., Smith, R., and Kuhlemeier, C. (2013). Interaction between meristem tissue layers controls phyllotaxis. Dev Cell 26: 616–628.
Google Scholar: Author Only Title Only Author and Title

Kim, D., Langmead, B., and Salzberg, S.L. (2015). HISAT: a fast spliced aligner with low memory requirements. Nat Methods 12: 357–360.
Google Scholar: Author Only Title Only Author and Title

Kostyun, J.L., Gibson, M.J.S., King, C.M., and Moyle, L.C. (2019). A simple genetic architecture and low constraint allow rapid floral evolution in a diverse and recently radiating plant genus. New Phytol 223: 1009–1022.
Google Scholar: Author Only Title Only Author and Title

Krieger, G., Lupo, O., Wittkopp, P., and Barkai, N. (2022). Evolution of transcription factor binding through sequence variations and turnover of binding sites. Genome Res 32: 1099–1111.
Google Scholar: Author Only Title Only Author and Title

van der Krol, A.R., Brunelle, A., Tsuchimoto, S., and Chua, N.H. (1993). Functional analysis of petunia floral homeotic MADS box gene pMADS1. Genes Dev 7: 1214–1228.
Google Scholar: Author Only Title Only Author and Title

Kutschera, U. and Niklas, K.J. (2007). The epidermal-growth-control theory of stem elongation: an old and a new perspective. J. Plant Physiol. 164: 1395–1409.
Google Scholar: Author Only Title Only Author and Title

Lassmann, T. (2019). Kalign 3: multiple sequence alignment of large data sets. Bioinformatics 36: 1928–1929.
Google Scholar: Author Only Title Only Author and Title

Liao, Y., Smyth, G.K., and Shi, W. (2014). featureCounts: an efficient general purpose program for assigning sequence reads to genomic features. Bioinformatics 30: 923–930.
Google Scholar: Author Only Title Only Author and Title

Love, M.I., Huber, W., and Anders, S. (2014). Moderated estimation of fold change and dispersion for RNA-seq data with DESeq2. Genome Biol 15: 550.
Google Scholar: Author Only Title Only Author and Title

Lu, P., Porat, R., Nadeau, J.A., and O'Neill, S.D. (1996). Identification of a meristem L1 layer-specific gene in Arabidopsis that is expressed during embryonic pattern formation and defines a new class of homeobox genes. Plant Cell 8: 2155–2168.
Google Scholar: Author Only Title Only Author and Title

Madeira, F., Pearce, M., Tivey, A.R.N., Basutkar, P., Lee, J., Edbali, O., Madhusoodanan, N., Kolesnikov, A., and Lopez, R. (2022). Search and sequence analysis tools services from EMBL-EBI in 2022. Nucleic Acids Res 50: W276–W279.
Google Scholar: Author Only Title Only Author and Title

Martin, M. (2011). Cutadapt removes adapter sequences from high-throughput sequencing reads. EMBnet.journal 17: 10–12.
Google Scholar: Author Only Title Only Author and Title

Mayor, C., Brudno, M., Schwartz, J.R., Poliakov, A., Rubin, E.M., Frazer, K.A., Pachter, L.S., and Dubchak, I. (2000). VISTA: visualizing global DNA sequence alignments of arbitrary length. Bioinformatics 16: 1046–1047.
Google Scholar: Author Only Title Only Author and Title

McHale, N.A. and Marcotrigiano, M. (1998). LAM1 is required for dorsoventrality and lateral growth of the leaf blade in Nicotiana. Development 125: 4235–4243.
Google Scholar: Author Only Title Only Author and Title

Melzer, R., Verelst, W., and Theissen, G. (2009). The class E floral homeotic protein SEPALLATA3 is sufficient to loop DNA in 'floral quartet'-like complexes in vitro. Nucleic Acids Res. 37: 144–157.
Google Scholar: Author Only Title Only Author and Title

Meyerowitz, E.M. (1997). Genetic control of cell division patterns in developing plants. Cell 88: 299–308.
Google Scholar: Author Only Title Only Author and Title

Morel, P., Chambrier, P., Boltz, V., Chamot, S., Rozier, F., Rodrigues Bento, S., Trehin, C., Monniaux, M., Zethof, J., and Vandenbussche, M. (2019). Divergent Functional Diversification Patterns in the SEP/AGL6/AP1 MADS-Box Transcription Factor Superclade. Plant Cell 31: 3033–3056.
Google Scholar: Author Only Title Only Author and Title

Morel, P., Heijmans, K., Rozier, F., Zethof, J., Chamot, S., Bento, S.R., Vialette-Guiraud, A., Chambrier, P., Trehin, C., and Vandenbussche, M. (2017). Divergence of the Floral A-Function between an Asterid and a Rosid Species. Plant Cell 29: 1605–1621.
Google Scholar: Author Only Title Only Author and Title

Moyroud, E. and Glover, B.J. (2017). The Evolution of Diverse Floral Morphologies. Curr. Biol. 27: R941–R951.
Google Scholar: Author Only Title Only Author and Title

Perbal, M.C., Haughn, G., Saedler, H., and Schwarz-Sommer, Z. (1996). Non-cell-autonomous function of the Antirrhinum floral homeotic proteins DEFICIENS and GLOBOSA is exerted by their polar cell-to-cell trafficking. Development 122: 3433–3441.
Google Scholar: Author Only Title Only Author and Title

Purugganan, M.D., Rounsley, S.D., Schmidt, R.J., and Yanofsky, M.F. (1995). Molecular evolution of flower development: diversification of the plant MADS-box regulatory gene family. Genetics 140: 345–356.
Google Scholar: Author Only Title Only Author and Title

Quattrocchio, F., Wing, J., van der Woude, K., Souer, E., de Vetten, N., Mol, J., and Koes, R. (1999). Molecular analysis of the anthocyanin2 gene of petunia and its role in the evolution of flower color. Plant Cell 11: 1433–1444.
Google Scholar: Author Only Title Only Author and Title

Quattrocchio, F., Wing, J.F., Leppen, H.T.C., Mol, J.N.M., and Koes, R.E. (1993). Regulatory Genes Controlling Anthocyanin Pigmentation Are Functionally Conserved among Plant Species and Have Distinct Sets of Target Genes. Plant Cell 5: 1497–1512.
Google Scholar: Author Only Title Only Author and Title

Quattrocchio, F., Wing, J.F., van der Woude, K., Mol, J.N., and Koes, R. (1998). Analysis of bHLH and MYB domain proteins: species-specific regulatory differences are caused by divergent evolution of target anthocyanin genes. Plant J 13: 475–488.
Google Scholar: Author Only Title Only Author and Title

Reale, L., Porceddu, A., Lanfaloni, L., Moretti, C., Zenoni, S., Pezzotti, M., Romano, B., and Ferranti, F. (2002). Patterns of cell division and expansion in developing petals of Petunia hybrida. Sex Plant Reprod 15: 123–132.
Google Scholar: Author Only Title Only Author and Title

Reck-Kortmann, M., Silva-Arias, G.A., Segatto, A.L.A., Mader, G., Bonatto, S.L., and de Freitas, L.B. (2014). Multilocus phylogeny reconstruction: new insights into the evolutionary history of the genus Petunia. Mol Phylogenet Evol 81: 19–28.
Google Scholar: Author Only Title Only Author and Title

Ren, H., Dang, X., Cai, X., Yu, P., Li, Y., Zhang, S., Liu, M., Chen, B., and Lin, D. (2017). Spatio-temporal orientation of microtubules controls conical cell shape in Arabidopsis thaliana petals. PLOS Genetics 13: e1006851.
Google Scholar: Author Only Title Only Author and Title

Riechmann, J.L., Krizek, B.A., and Meyerowitz, E.M. (1996a). Dimerization specificity of Arabidopsis MADS domain homeotic proteins APETALA1, APETALA3, PISTILLATA, and AGAMOUS. Proc Natl Acad Sci U S A 93: 4793–4798.
Google Scholar: Author Only Title Only Author and Title

Riechmann, J.L., Wang, M., and Meyerowitz, E.M. (1996b). DNA-binding properties of Arabidopsis MADS domain homeotic proteins APETALA1, APETALA3, PISTILLATA and AGAMOUS. Nucleic Acids Res 24: 3134–3141.
Google Scholar: Author Only Title Only Author and Title

Rijpkema, A.S., Royaert, S., Zethof, J., Weerden, G. van der, Gerats, T., and Vandenbussche, M. (2006). Analysis of the Petunia TM6 MADS Box Gene Reveals Functional Divergence within the DEF/AP3 Lineage. The Plant Cell 18: 1819–1832.
Google Scholar: Author Only Title Only Author and Title

Sandelin, A., Alkema, W., Engström, P., Wasserman, W.W., and Lenhard, B. (2004). JASPAR: an open-access database for eukaryotic transcription factor binding profiles. Nucleic Acids Res 32: D91-94.
Google Scholar: Author Only Title Only Author and Title

Satina, S. and Blakeslee, A.F. (1941). Periclinal Chimeras in Datura Stramonium in Relation to Development of Leaf and Flower. American Journal of Botany 28: 862–871.
Google Scholar: Author Only Title Only Author and Title

Satina, S., Blakeslee, A.F., and Avery, A.G. (1940). Demonstration of the Three Germ Layers in the Shoot Apex of Datura by Means of Induced Polyploidy in Periclinal Chimeras. American Journal of Botany 27: 895–905.
Google Scholar: Author Only Title Only Author and Title

Savaldi-Goldstein, S., Peto, C., and Chory, J. (2007). The epidermis both drives and restricts plant shoot growth. Nature 446: 199–202.
Google Scholar: Author Only Title Only Author and Title

Scheres, B. (2001). Plant cell identity. The role of position and lineage. Plant Physiol 125: 112–114.
Google Scholar: Author Only Title Only Author and Title

Schmidt, D. et al. (2010). Five-vertebrate ChIP-seq reveals the evolutionary dynamics of transcription factor binding. Science 328: 1036–1040.
Google Scholar: Author Only Title Only Author and Title

Schwarz-Sommer, Z., Hue, I., Huijser, P., Flor, P.J., Hansen, R., Tetens, F., Lönnig, W.E., Saedler, H., and Sommer, H. (1992). Characterization of the Antirrhinum floral homeotic MADS-box gene deficiens: evidence for DNA binding and autoregulation of its persistent expression throughout flower development. EMBO J. 11: 251–263.
Google Scholar: Author Only Title Only Author and Title

Schwarz-Sommer, Z., Huijser, P., Nacken, W., Saedler, H., and Sommer, H. (1990). Genetic Control of Flower Development by Homeotic Genes in Antirrhinum majus. Science 250: 931–936.
Google Scholar: Author Only Title Only Author and Title

Sierro, N., Battey, J.N.D., Ouadi, S., Bakaher, N., Bovet, L., Willig, A., Goepfert, S., Peitsch, M.C., and Ivanov, N.V. (2014). The tobacco genome sequence and its comparison with those of tomato and potato. Nat Commun 5: 3833.
Google Scholar: Author Only Title Only Author and Title

Silva, C.S., Puranik, S., Round, A., Brennich, M., Jourdain, A., Parcy, F., Hugouvieux, V., and Zubieta, C. (2015). Evolution of the Plant Reproduction Master Regulators LFY and the MADS Transcription Factors: The Role of Protein Structure in the Evolutionary Development of the Flower. Front Plant Sci 6: 1193.
Google Scholar: Author Only Title Only Author and Title

Slater, G.S.C. and Birney, E. (2005). Automated generation of heuristics for biological sequence comparison. BMC Bioinformatics 6: 31.
Google Scholar: Author Only Title Only Author and Title

Solomon, E.R., Caldwell, K.K., and Allan, A.M. (2021). A novel method for the normalization of ChIP-qPCR data. MethodsX 8: 101504.
Google Scholar: Author Only Title Only Author and Title

Spelt, C., Quattrocchio, F., Mol, J.N.M., and Koes, R. (2000). anthocyanin1 of Petunia Encodes a Basic Helix-Loop-Helix Protein That Directly Activates Transcription of Structural Anthocyanin Genes. The Plant Cell 12: 1619–1631.
Google Scholar: Author Only Title Only Author and Title

Stewart, R.N. and Burk, L.G. (1970). Independence of Tissues Derived from Apical Layers in Ontogeny of the Tobacco Leaf and Ovary. American Journal of Botany 57: 1010–1016.
Google Scholar: Author Only Title Only Author and Title

Stormo, G.D. (2013). Modeling the specificity of protein-DNA interactions. Quant Biol 1: 115–130.
Google Scholar: Author Only Title Only Author and Title

Stuurman, J., Hoballah, M.E., Broger, L., Moore, J., Basten, C., and Kuhlemeier, C. (2004). Dissection of floral pollination syndromes in Petunia. Genetics 168: 1585–1599.
Google Scholar: Author Only Title Only Author and Title

Takatani, S., Verger, S., Okamoto, T., Takahashi, T., Hamant, O., and Motose, H. (2020). Microtubule Response to Tensile Stress Is Curbed by NEK6 to Buffer Growth Variation in the Arabidopsis Hypocotyl. Curr Biol 30: 1491-1503.e2.
Google Scholar: Author Only Title Only Author and Title

Terry, M.I., Pérez-Sanz, F., Díaz-Galián, M.V., Pérez de Los Cobos, F., Navarro, P.J., Egea-Cortines, M., and Weiss, J. (2019). The Petunia CHANEL Gene is a ZEITLUPE Ortholog Coordinating Growth and Scent Profiles. Cells 8.
Google Scholar: Author Only Title Only Author and Title

Theißen, G., Kim, J.T., and Saedler, H. (1996). Classification and phylogeny of the MADS-box multigene family suggest defined roles of MADS-box gene subfamilies in the morphological evolution of eukaryotes. J Mol Evol 43: 484–516.
Google Scholar: Author Only Title Only Author and Title

Tilney-Bassett, R.A.E. (1986). Plant chimeras (E. Arnold: London ; Baltimore, Md., U.S.A).
Google Scholar: Author Only Title Only Author and Title

Tornielli, G., Koes, R., and Quattrocchio, F. (2009). The Genetics of Flower Color. In Petunia: Evolutionary, Developmental and Physiological Genetics, T. Gerats and J. Strommer, eds (Springer: New York, NY), pp. 269–299.
Google Scholar: Author Only Title Only Author and Title

Tröbner, W., Ramirez, L., Motte, P., Hue, I., Huijser, P., Lönnig, W.E., Saedler, H., Sommer, H., and Schwarz-Sommer, Z. (1992). GLOBOSA: a homeotic gene which interacts with DEFICIENS in the control of Antirrhinum floral organogenesis. EMBO J 11: 4693–4704.
Google Scholar: Author Only Title Only Author and Title

Urbanus, S.L., Dinh, Q.D.P., Angenent, G.C., and Immink, R.G.H. (2010a). Investigation of MADS domain transcription factor

dynamics in the floral meristem. Plant Signal Behav 5: 1260–1262.
Google Scholar: Author Only Title Only Author and Title

Urbanus, S.L., Martinelli, A.P., Dinh, Q.D.P., Aizza, L.C.B., Dornelas, M.C., Angenent, G.C., and Immink, R.G.H. (2010b). Intercellular transport of epidermis-expressed MADS domain transcription factors and their effect on plant morphology and floral transition. Plant J 63: 60–72.
Google Scholar: Author Only Title Only Author and Title

Vandenbussche, M., Horstman, A., Zethof, J., Koes, R., Rijpkema, A.S., and Gerats, T. (2009). Differential recruitment of WOX transcription factors for lateral development and organ fusion in Petunia and Arabidopsis. Plant Cell 21: 2269–2283.
Google Scholar: Author Only Title Only Author and Title

Vandenbussche, M., Janssen, A., Zethof, J., van Orsouw, N., Peters, J., van Eijk, M.J.T., Rijpkema, A.S., Schneiders, H., Santhanam, P., de Been, M., van Tunen, A., and Gerats, T. (2008). Generation of a 3D indexed Petunia insertion database for reverse genetics. Plant J 54: 1105–1114.
Google Scholar: Author Only Title Only Author and Title

Vandenbussche, M., Zethof, J., Royaert, S., Weterings, K., and Gerats, T. (2004). The duplicated B-class heterodimer model: whorl-specific effects and complex genetic interactions in Petunia hybrida flower development. Plant Cell 16: 741–754.
Google Scholar: Author Only Title Only Author and Title

Venail, J., Dell'olivo, A., and Kuhlemeier, C. (2010). Speciation genes in the genus Petunia. Philos Trans R Soc Lond B Biol Sci 365: 461–468.
Google Scholar: Author Only Title Only Author and Title

de Vetten, N., Quattrocchio, F., Mol, J., and Koes, R. (1997). The an11 locus controlling flower pigmentation in petunia encodes a novel WD-repeat protein conserved in yeast, plants, and animals. Genes Dev 11: 1422–1434.
Google Scholar: Author Only Title Only Author and Title

Vincent, C.A., Carpenter, R., and Coen, E.S. (2003). Interactions between gene activity and cell layers during floral development. The Plant Journal 33: 765–774.
Google Scholar: Author Only Title Only Author and Title

de Vlaming, P., Gerats, A.G.M., Wiering, H., Wijsman, H.J.W., Cornu, A., Farcy, E., and Maizonnier, D. (1984). Petunia hybrida: A short description of the action of 91 genes, their origin and their map location. Plant Mol Biol Rep 2: 21–42.
Google Scholar: Author Only Title Only Author and Title

Wuest, S.E., O'Maoileidigh, D.S., Rae, L., Kwasniewska, K., Raganelli, A., Hanczaryk, K., Lohan, A.J., Loftus, B., Graciet, E., and Wellmer, F. (2012). Molecular basis for the specification of floral organs by APETALA3 and PISTILLATA. Proc. Natl. Acad. Sci. U.S.A. 109: 13452–13457.
Google Scholar: Author Only Title Only Author and Title

Yadav, R.K., Tavakkoli, M., Xie, M., Girke, T., and Reddy, G.V. (2014). A high-resolution gene expression map of the Arabidopsis shoot meristem stem cell niche. Development 141: 2735–2744.
Google Scholar: Author Only Title Only Author and Title

Zenoni, S., Reale, L., Tornielli, G.B., Lanfaloni, L., Porceddu, A., Ferrarini, A., Moretti, C., Zamboni, A., Speghini, A., Ferranti, F., and Pezzotti, M. (2004). Downregulation of the Petunia hybrida alpha-expansin gene PhEXP1 reduces the amount of crystalline cellulose in cell walls and leads to phenotypic changes in petal limbs. Plant Cell 16: 295–308.
Google Scholar: Author Only Title Only Author and Title

Zhang, B., Xu, X., Huang, R., Yang, S., Li, M., and Guo, Y. (2021). CRISPR/Cas9-mediated targeted mutation reveals a role for AN4 rather than DPL in regulating venation formation in the corolla tube of Petunia hybrida. Hortic Res 8: 116.
Google Scholar: Author Only Title Only Author and Title

Zhao, F. et al. (2020). Microtubule-Mediated Wall Anisotropy Contributes to Leaf Blade Flattening. Curr Biol 30: 3972-3985.e6.
Google Scholar: Author Only Title Only Author and Title